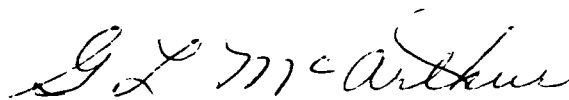


Final Report

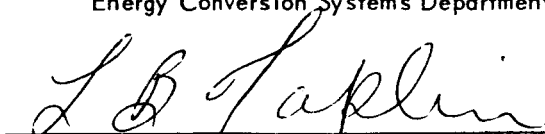
**ANALYTICAL STUDY OF
THE FEASIBILITY OF A PNEUMATIC
NEUTRON FLUX DETECTOR**

Prepared Under
the Direction of:



G. L. McArthur, Assistant Head
Energy Conversion Systems Department

Approved by:



L. B. Taplin, Manager
Energy Conversion and Dynamic Controls Laboratory

Prepared for

NATIONAL AERONAUTICS AND SPACE ADMINISTRATION

May 1965

CONTRACT NAS 3-6207

Technical Management
NASA Lewis Research Center
Cleveland, Ohio
Nuclear Rocket Technology Office
John C. Liwosz

By

The Bendix Corporation
Research Laboratories Division
Southfield, Michigan

TABLE OF CONTENTS

	<u>Page</u>
SECTION 1 - CONCLUSIONS AND RECOMMENDATIONS	1-1
1.1 Results and Conclusions	1-1
1.2 Recommendations	1-2
SECTION 2 - INTRODUCTION	2-1
2.1 Purpose of Investigation	2-1
2.1.1 Present Methods of Measuring Neutron Flux	2-2
2.1.2 Advantages of Fluid State Detectors	2-2
2.2 Scope of Investigation	2-3
2.2.1 Desired Performance of Pneumatic Neutron Flux Detectors	2-3
2.2.2 General Approach and Significance of Results	2-4
SECTION 3 - PRELIMINARY STUDIES	3-1
3.1 The Initial Concept	3-1
3.2 The Vortex Amplifier	3-2
3.3 The Magnetohydrodynamic Sensor	3-2
3.4 Preliminary Analysis - Magnetofluidynamic and Electrofluidynamic Pressure Generators	3-3
SECTION 4 - EFD PUMP ANALYSIS	4-1
4.1 General Discussion	4-1
4.2 Theoretical Analysis	4-2
4.2.1 Neutron Conversion to Current Density	4-2
4.2.2 The Working Fluid	4-3
4.2.3 Theory of the Gaseous EFD Hydrogen Pump	4-6
4.2.4 The Effects of Recombination, Diffusion, and Space Charge	4-9
SECTION 5 - VORTEX AMPLIFIER ANALYSIS	5-1
5.1 Basic Principles of Vortex Amplifiers	5-1
5.1.1 Description of Vortex Amplifier	5-1
5.1.2 Calculation of the Pressure Drop Across a Vortex in an Inviscid Ideal Gas	5-2
5.1.3 Actual Vortex Amplifier Performance	5-5

	<u>Page</u>
5.2 Factors Affecting Vortex Amplifier Pressure Gains and Outputs	5-11
5.2.1 Temperature Sensitivity	5-11
5.2.2 Supply Pressure Sensitivity	5-16
5.2.3 Effect of Control Port Area on Vortex Pressure Amplifier Gain	5-18
5.2.4 Effect of Pickoff	5-22
5.3 Logarithmic Output and Range Characteristics	5-24
5.3.1 Estimate of Neutron Sensor High Gain Amplifier Gains and Flows	5-24
5.3.2 Theoretical Gains Required to Obtain a Logarithmic Output	5-26
5.3.3 Logarithmic Characteristics of High Gain Vortex Amplifiers	5-27
5.4 Dynamic Response Characteristics	5-32
5.4.1 Estimate of High Gain Vortex Amplifier Dynamics	5-32
5.4.2 Estimate of Dynamics Downstream of High Gain Vortex Amplifier	5-36
5.5 Noise Characteristics	5-41
SECTION 6 - SENSOR SYSTEM ANALYSIS	6-1
6.1 Description of System	6-1
6.1.1 EFD Pump	6-1
6.1.2 Vortex Amplifiers	6-2
6.1.3 Complete System	6-4
6.2 Nuclear Studies	6-7
6.2.1 Gamma Shielding	6-7
6.2.2 Gamma Heating	6-7
6.2.3 Moderator	6-9
6.2.4 Neutron Conversion Coating	6-11

	<u>Page</u>
6.3 System Dynamic Response	6-13
6.4 System Range	6-13
6.5 System Accuracy	6-14
6.6 System Weight and Gas Consumption Estimates	6-16
 APPENDIX A - NOTATIONS	 A-1

LIST OF ILLUSTRATIONS

<u>Figure No.</u>	<u>Title</u>	<u>Page</u>
2-1	Reactor Control System	2-1
3-1	Schematic Diagram - Magnetofluidynamic Vortex Concept	3-1
3-2	Schematic Configuration of Rectilinear Electrofluidynamic Pressure Generator	3-5
5-1	Vortex Amplifier Schematic	5-1
5-2	Conventional Representation of Vortex Amplifiers	5-2
5-3	Output Performance of a One Inch Vortex Amplifier	5-6
5-4	Typical Performance of Two and Three Inch Vortex Amplifiers with Internal Pickoffs at 30 Psig Supply Pressure	5-6
5-5	Effect of Supply Pressure on Vortex Pressure Amplifier Performance	5-10
5-6	Flows through Three Inch High Gain Pressure Amplifier at 30 Psig Supply Pressure	5-10
5-7	Effect of Temperature of One Inch Vortex Pressure Amplifier at 75 Psig Supply Pressure	5-13
5-8	Effect of Reynolds Number on Maximum Pressure Gain of a One Inch Diameter Vortex Amplifier	5-15
5-9	Relation Between \dot{w}_o and p_{oi} for Vortex Amplifiers of Various Diameters at $p_s = 44.7$ Psia	5-20
5-10	Logarithmic Characteristics of a Three Inch Vortex Amplifier with a 0.0075 Psi Bias Pressure	5-28
5-11	Approach to Logarithmic Vortex Amplifier	5-29
5-12	Approximation of Logarithmic Function	5-32
5-13	Cascaded Vortex Amplifiers	
6-1	Ion Pump Perspective	6-1
6-2	Pneumatic Neutron Flux Detector Schematic	6-3
6-3	Ion Pump-Vortex Amplifier Assembly	6-5
6-4	Shield and Moderator Schematic	6-6

LIST OF TABLES

<u>Table No.</u>	<u>Title</u>	<u>Page</u>
5-1	Vortex Amplifier Diameters	5-7
5-2	Estimates of Flow Demands for High Gain Amplifier with $C_{dc}A_c = 0.088 \text{ in}^2$	5-26
6-1	Desired Vortex Amplifier Gains for Linear Ion Pump	6-4
6-2	Moderating Characteristics of Various Materials	6-9

ANALYTICAL STUDY OF THE FEASIBILITY OF A PNEUMATIC NEUTRON FLUX DETECTOR

ABSTRACT

16901

An analytical study to determine the feasibility of developing a pneumatic neutron flux detector has been conducted. The concept examined consisted of an electrofluidynamic pump for converting thermal neutron flux to a pneumatic pressure signal which is amplified by a logarithmic vortex amplifier. At least five decades of neutron flux from 10^7 to 10^{12} neutrons/cm²-sec can be detected. Response times (95 percent final value) approaching 0.06 sec can be achieved. Quantitative definition of accuracy requires additional experimental evaluation. Methods of gamma compensation, sensitivity to temperature changes, and capability of meeting operational modes were also considered in this feasibility analysis. A conceptual design of a feasible neutron flux detector is provided.

Author

SUMMARY

The objective of the investigation described in this report was to conduct an analytical study to determine the feasibility of developing a pneumatic neutron flux detector suitable for use in a nuclear rocket. The neutron flux detector is to have a response time (63 percent output) of 0.02 sec at flux levels greater than 10^7 neutrons/cm² sec and 1 sec at the lower flux levels. The desired range is 10 decades of fast neutron flux (2.9 Mev) from 10^2 to 10^{12} neutrons/cm² sec. The desired accuracy is ± 10 percent of the indicated flux over the ambient temperature range of 200 - 800°R and under 7 g from 10 to 2000 cps vibration. A logarithmic output is required. The device is to be compensated for gamma flux up to 5×10^9 ergs/gm(c)hr and is to be capable of operating under restart conditions.

The original concept pursued was a combination of the magneto-fluiddynamic effect and the vortex amplifier. In this approach, thermal neutron flux produces ionizing particles which ionize the working fluid in the vortex amplifier, and a vortex flow is produced by the magneto-fluiddynamic interaction between the ionized fluid and crossed magnetic and electric fields. The output pressure of the vortex amplifier is a function of the vortex flow and hence the neutron flux. The configuration is fundamentally that of an electric motor with a fluid rotor.

After a comparison of fluids that might be suitable as working media for the neutron flux detector, hydrogen was selected both for its desirable physical characteristics and its availability.

Analysis performed early in the investigation revealed that a greater physical effect could be produced by electrofluiddynamic pumping rather than by magnetofluiddynamic pumping; thus, the electrofluiddynamic effect was selected for the feasibility study. Production of electro-fluiddynamic forces in the annulus of a vortex amplifier leads to difficulties in design and fabrication; so the neutron sensor concept was changed to utilize an electrofluiddynamic pump external to the vortex amplifier. This pump modulates the control flow as a function of gas ionization produced by thermal neutron flux. The control flow produces a vortex flow in the vortex amplifier, creating an output pressure change which is significantly greater than the pressure change at the control flow inlet.

Vortex amplifier pressure gains (change of output pressure divided by change in control port differential pressure) in the range of 3000 to 6200 are feasible. Vortex amplifier noise levels are expected to be sufficiently low so that changes in the electrofluidynamic pump output pressure as low as 10^{-5} psi can be detected. This corresponds to a thermal neutron flux of 1.2×10^6 neutrons/cm² sec indicating that at least five decades of moderated fast neutron flux below 10^{12} neutrons/cm² sec can be detected. A logarithmic function can be approximated to within 10 percent of the output range with the greatest deviation at the lowest input.

It has been concluded that the desired dynamic response can be obtained. However, it is expected that it will be marginal if the hydrogen working fluid is at 200°R. Compensation for at least 90 percent of the gamma ionization can be obtained with a fixed voltage. Quantitative definition of accuracy requires additional experimental evaluation. Areas which should be covered in such an investigation include the temperature sensitivity of the device and methods of temperature compensation and verification of the nonlinear characteristics of both vortex amplifiers and the electrofluidynamic pump.

Moderator will be required for the pneumatic neutron sensor, as for the more conventional counter types; however, the shielding required will be significantly less. Within the operating cycles specified, no progressive null shift would be expected in contrast with devices based on materials subject to changes from radiation.

The potential of the pneumatic neutron detector as a radiation-insensitive sensor for reactor monitoring and control makes a development effort to experimentally verify the feasibility very worthwhile. In addition to verifying the performance predicted during the feasibility study, the experimental effort should be directed toward the collection of design data, removing existing limitations and generally advancing the state of the art of neutron detection.

SECTION 1

CONCLUSIONS AND RECOMMENDATIONS

1.1 RESULTS AND CONCLUSIONS

Analyses performed in this four month study program show that it is feasible to develop a fluid state neutron detector suitable for use in the control of a nuclear rocket. Electrofluidynamic rather than magnetofluidynamic operating principles were determined by detailed analysis to be most appropriate for converting neutron flux to pneumatic pressure. The conceptual design is a series arrangement of an electrofluidynamic pump and a vortex pressure amplifier. Neutron flux produces ionization in the working fluid which passes through an electrostatic field in the pump. Ions and electrons are accelerated by the electrostatic field and they (principally the ions) impart momentum to gas molecules through collisions, thereby raising the pressure of the gas entering the vortex amplifier control port. This pressure is amplified to a suitable output by a very sensitive vortex pressure amplifier. A similar pump connected in series opposition by reversing the polarity of the electrostatic field provides compensation for gamma rays.

The predicted range of the detector is five decades covered by two vortex amplifiers with overlapping ranges. The prediction is based on present capabilities of fluid-state amplifiers and conservative estimates of breakdown phenomenon in high pressure hydrogen which is largely unknown. Additional experimental data will permit a determination of how far the range can be extended. Extending the range just two more decades will enable the sensor to cover the restart range even though it may not cover the full start-up range. Initial cold startup will in all probability be performed open loop anyway; so the lower portion of the power range could be measured with conventional neutron counters. They would not be subjected to severe radiation in that range and would not have to be used for restart.

Response time (time constant) predicted for the system is approximately the same as that specified, even at the lowest temperature level. The high hydrogen flow rates and fast responding vortex amplifier are largely responsible for achieving the fast response. This objective is considered one of the most important since one of the purposes for the neutron flux loop in the control system is to augment the slower responding temperature loop and thereby enable rapid changes in reactor

power level in response to flow changes or thrust demands. Even at the lower power ranges, the response is expected to be within the time specified.

Accuracy of the system cannot be fully assessed because it depends largely on how well the total sensor approximates a logarithmic characteristic and on its sensitivity to changes in environmental conditions. The overall characteristic of the sensor can be shaped to a certain extent by tailoring the design and operating point of the vortex amplifier to the EFD pump. The vortex amplifier output varies from linear to logarithmic over various portions of its range. The pump characteristic in theory varies as the two-thirds power of the flux. A realistic evaluation of the characteristic and hence the accuracy can be made only by an experimental determination.

Weight and size of the complete neutron sensor exclusive of any shielding or moderator is 6.7 pounds and 75 cubic inches. Some gamma shielding is required to insure adequate gamma compensation on a re-start condition. Approximately 6 half-thicknesses of lead are provided for that purpose.

Moderator material recommended is beryllium because of its low weight and volume. Graphite or polystyrene are other choices which could be used without significant attenuation of the neutron flux at the detector.

Nuclear heating is not a problem in the sensor itself because of its low mass and large hydrogen flow rate. Nuclear heating in the moderator and shield does not pose a problem since they are physically isolated from the sensor, do not depend on maintaining close tolerances of physical properties and can be cooled to whatever degree necessary by low temperature hydrogen gas.

Boron-10 is recommended as the neutron sensitive coating because of its greater efficiency for producing ionization from thermal neutrons. Coating Boron-10 on the internal walls of the pump can be accomplished within existing state of the art technology; so it will not present any special difficulty.

1.2 RECOMMENDATIONS

The feasibility of a fluid-state neutron sensor operating over five decades has been established analytically, but there are a number of assumptions which must be verified experimentally before an

operational hardware development program can be initiated. Data on the behavior of weakly ionized hydrogen at low electric fields and high pressures are virtually nonexistent; so extensive extrapolations were necessary in the performance of this study. The prospects for extending the range of the sensor to lower decades are promising but experimental data on breakdown phenomena, charge collection and wall charging are needed before these extensions can be considered realistically. Similarly meaningful predictions of output characteristic and sensor accuracy can be made only after suitable experimental data have been generated. Therefore it is recommended that a second phase of the EFD fluid state neutron sensor be carried out with the objectives of experimentally demonstrating the feasibility of the five decade sensor, determining the limits of operation and sensitivity to the environment, and obtaining the design data to optimize performance and extend the range of operation.

In addition to this experimental effort aimed at verifying sensor performance and obtaining design data, there are a number of critical problems which require more thorough investigation to permit optimizing the design of the sensor and it is recommended that they also be performed in this second phase of the program. Completion of this experimental and critical problem investigation will provide the necessary background and design data to permit the detailed development of a prototype EFD neutron sensor in a subsequent phase.

Outlined below is an experimental program which has been devised for the purpose of (1) verifying the assumptions made in the analytical study, (2) determining the limits of operation, (3) investigating environmental effects and (4) obtaining the design data to permit extending the range of operation and optimizing performance. The specific tasks required to demonstrate the performance of the EFD fluid state neutron sensor are itemized below:

Task 1 - EFD Pump Investigation

- 1-A Design and construct an EFD pump, incorporating suitable dimensional adjustments and being suitable for testing in a low gas capacity recirculating system.

- 1-B Design and construct a test system utilizing corona ionization to evaluate the EFD pump.

Factors to be investigated are:

- (a) Maximum voltage and grid separations (pump stage length) for which reliable operation can be sustained without spontaneous arc generation.
- (b) Evaluate the effects of stacked tube or honeycomb pore size to optimize ion collection efficiency.

- 1-C Modify test system to test in an X-ray field for space generation of charge and for evaluation of gamma compensation (Using the corona generator as a signal on the X-ray background).

- 1-D Evaluate the EFD pump behavior in a neutron field either separate from or combined with the vortex amplifier.

Task 2 - Vortex Amplifier Investigation

- 2-A Design, fabricate and test a vortex amplifier aimed at the performance required for the fluid state neutron flux detector. The critical problem areas to be investigated are:

- (a) Temperature compensation
- (b) Logarithmic output characteristics
- (c) Sensitivity improvement and range extension
- (d) Response characteristics.

- 2-B Design, fabricate and test breadboard fluid state networks, coupling elements to investigate methods of:

- (a) Extending sensor range
- (b) Providing pressure regulation
- (c) Compensating for temperature changes where this cannot be provided in a single element
- (d) Improving logarithmic output characteristics.

Task 3 - EFD Pump/Vortex Amplifier Matching

- 3-A Design, fabricate and test a breadboard sensor incorporating an EFD Pump and high performance vortex amplifier. The preliminary testing of this breadboard will be directed toward assessing compatibility, establishing and/or verifying design criteria, gathering design data and evaluating sensor potential.
- 3-B Perform the design analysis and prepare a preliminary design of a prototype sensor system providing the supporting analysis and data concerning the expected performance of the sensor.

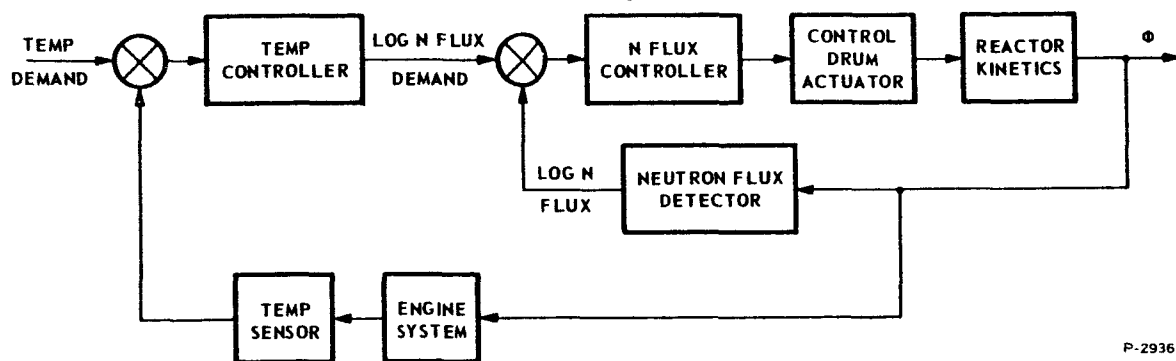
SECTION 2

INTRODUCTION

2.1 PURPOSE OF INVESTIGATION

All-pneumatic or, more generally, fluid state, control elements are presently being given serious consideration for controlling future nuclear rockets because of their potentially greater reliability in the severe environment surrounding the nuclear reactor. Because of the virtual absence of moving parts and exclusive use of extreme environment materials, fluid-state devices have much greater capability than electrical or electromechanical components for surviving the combined effects of nuclear radiation, cryogenic temperature, nuclear heating, acoustic noise, shock and vibration.

For the nuclear rocket, the neutron sensor is one of the key control components governing the feasibility of fluid-state nuclear rocket controls. Other fluid-state control components such as amplifiers, actuators, logic circuits and temperature and pressure sensors have been shown to be feasible for nuclear rocket control systems such as the one shown in the block diagram of Figure 2-1. A fluid-state neutron flux sensor compatible with the above-mentioned control elements is required before complete fluid-state controls can be fully realized. The purpose of this investigation is to determine by an analytical study the feasibility of developing such a fluid state neutron sensor which employs magnetofluidynamic or electrofluidynamic principles for continuously converting neutron flux to a fluid pressure or flow.



P-2936

Figure 2-1 - Reactor Control System

2.1.1 Present Methods of Measuring Neutron Flux

Present techniques for measuring neutron flux of the levels required by the specification use ionization chambers and neutron counters. Both techniques rely on the collection of electronic charge liberated by the interaction of gas atoms and heavy, charged particles which are released when neutrons are captured in neutron-absorbing materials. The output of the ionization chamber is an electrical current proportional to the impinging neutron flux. This chamber generally covers a range of five or six decades depending on the degree of compensation applied and the accuracy required. The signal requires amplification by electronic amplifiers to raise the level to that compatible with electrical control subsystems. A logarithmic characteristic is obtained by electronic shaping networks.

The neutron counter output is an electrical pulse for each ionizing event that occurs within the counter. The pulse repetition rate is proportional to the impinging neutron flux. This type of sensor also requires electronic amplification and covers five to six decades depending on the resolution of the electronic amplifiers and the accuracy requirements. A logarithmic characteristic is obtained by electronic pulse averaging and shaping networks.

In typical reactor installations, the total power range of 10 to 12 decades is covered by an overlapping combination of both types of neutron sensors. The neutron counter covers the lower 5 or 6 decades logarithmically and the ionization chamber logarithmically covers the upper 5 or 6 decades.

2.1.2 Advantages of Fluid State Detectors

One significant drawback of electrical sensors and amplifiers is their susceptibility to the radiation and temperature environment. High gamma radiation rates and high temperatures produce ionization in electrical cables and components as well as in the atmosphere surrounding these components. The resulting induced currents can be comparable to signal currents, thereby severely affecting the signal-to-noise ratio and appearing as an error in neutron flux. Fluid-state sensors are of course unaffected by such ionization in cables and components, which accounts for one of the potential advantages they enjoy.

The other important advantage of fluid-state detectors is that output signals are pneumatic and directly compatible with fluid-state control subsystems. Direct conversion of neutron flux to pneumatic pressure avoids the need of undesirable, and often unreliable, electric-to-pneumatic interfaces. This feature, combined with immunity to the severe environments, provides the incentive for undertaking this investigation.

2.2 SCOPE OF INVESTIGATION

2.2.1 Desired Performance of Pneumatic Neutron Flux Detectors

The feasibility of the pneumatic neutron flux detector was evaluated on the basis of several critical performance criteria and other instrument behavior requirements specified by the NASA, Lewis Research Center.

The most critical performance criterion is response time. For flux levels greater than 10^7 neutrons per cm^2 per second a response time of less than 0.02 second was specified (this was later clarified to mean a first-order time constant of 0.02 second). Below the flux level of 10^7 neutrons per cm^2 per second a response time of less than 1.0 second is deemed satisfactory.

The range of the detector, the second most critical performance criterion, should be ten (10) decades of fast neutron flux (2.9 Mev) from 10^2 to 10^{12} neutrons/ cm^2 sec. Preferably, this should be accomplished with a single sensor. However, a combination of overlapping sensors to cover the complete range is permissible.

The third performance criterion in order of importance is accuracy. The overall accuracy desired is ± 10 percent of the indicated flux while operating under the specified environment. This includes any inaccuracies caused by incomplete gamma compensation.

There are several other desirable features which were to be included as a part of the study. The device is to be compensated for gamma effects, especially as the gamma flux affects restart capability. It is desired that the device have a pneumatic output signal proportional to the logarithm of the neutron flux. The device should have a capability for twenty (20) minutes of continuous operation and for several shutdown and restart operations--total time of operation at full power up to one hour. Finally, electrical components are limited to simple electrodes and conductors for propagation of electrical or magnetic fields.

It is required that the detector be compatible with the environment. It is to be located above the reactor where the temperature will range from 200°R to 800°R. Vibration up to 7 g's (RMS) and over a frequency of 10 to 2000 cycles per second may be encountered.

2.2.2 General Approach and Significance of Results

The approach on the project was to separate the activities along the lines of the physical phenomena involved, with the investigation of the vortex amplifier characteristics and limitations constituting one task, and the neutron flux sensing and conversion to amplifier input forming the other. Those factors pertinent to this feasibility study were defined and evaluated.

The sensitivity of the vortex amplifier is a critical factor in that it influences the lowest detectable flux level of the sensor. This threshold is determined primarily by the "noise" generated in the system. Another portion of the amplifier investigation was directed toward the gain characteristics, the achievable range within the logarithmic output capability and response. High amplifier gain and high response are not compatible requirements and must be examined concurrently to achieve the optimum results. A near-logarithmic output is an inherent characteristic of vortex amplifiers over some portion of their operating curve. The range of the logarithmic operating curve is limited and more than one vortex amplifier is required to cover the range of the neutron sensor.

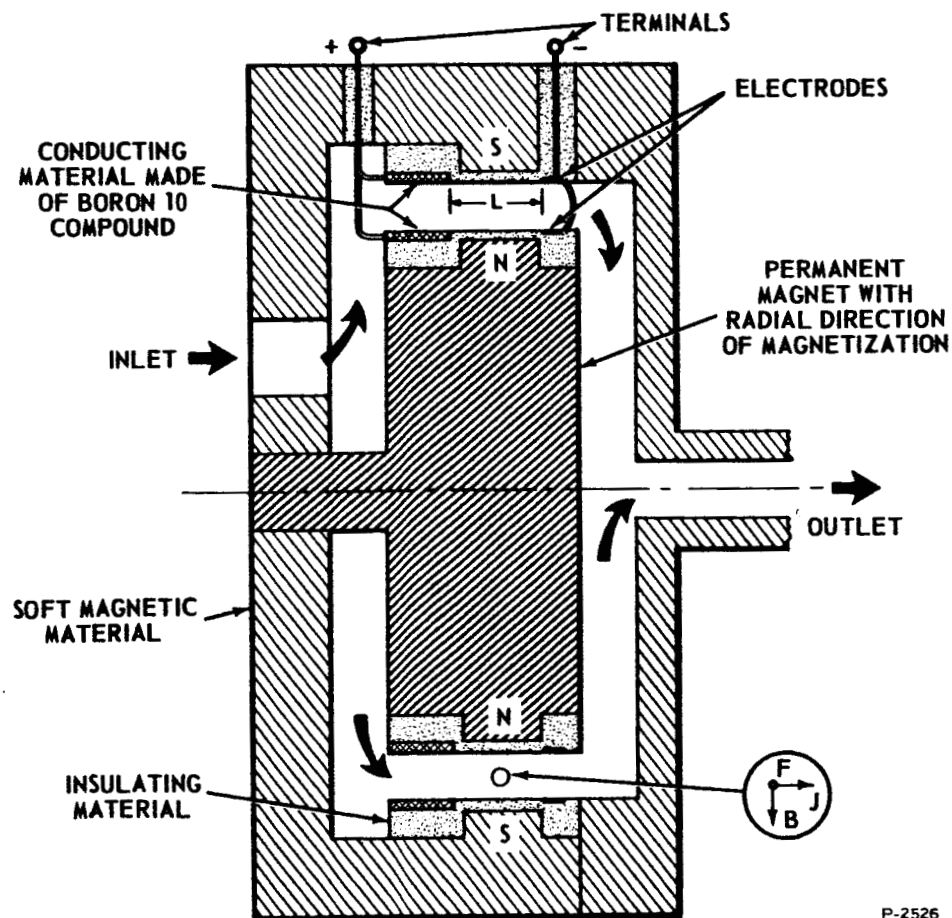
Two methods of capturing neutrons and converting their energy to pressure signal modulation were investigated. Both approaches involved the determination of the signal which one might expect from the minimum flux intensity. Throughout the study, the more conservative approach has been the rule. The magnitude of the signal which can be generated by the magnetofluidynamic technique is such that only the highest flux levels can be detected. The electrofluidynamic pump, on the other hand, offers the potential of measuring at least the upper five decades. Also, in the EFD concept, the gamma flux compensation is more easily accomplished. These studies on neutron energy conversion also included the requirements for moderator and the application of neutron conversion coatings in the EFD pump.

After the two separate EFD pump and vortex amplifier investigations proceeded far enough to be significant, the results were compared for compatibility and efforts redirected as required. For example, the sensitivity of the vortex amplifier was compared with the pressure signal capability of the EFD pump to determine the limiting factor. It was apparent that the entire range can not be measured without (1) reducing the noise level of the amplifier (increasing sensitivity) or (2) increasing pressure signal output from the pump. Both of these courses were re-examined to the degree permitted by the scope of this study. Similarly, the problems of design integration were evaluated to arrive at the design most suitable for the combination. A high performance pump may be self-defeating if it generates "noise" for the amplifier. Usually it is not necessary to sacrifice performance but rather only to recognize the need for compatibility during the design activity.

SECTION 3
PRELIMINARY STUDIES

3.1 THE INITIAL CONCEPT

The initial concept of the pneumatic neutron sensor proposed for this study was based upon two physical phenomena. The phenomenon of the vortex amplifier was utilized to magnify the effects of a change in tangential momentum produced by the magnetofluidynamic principle. This concept is shown schematically in Figure 3-1. For purposes of this discussion the two phenomena will be treated separately.



P-2526

Figure 3-1 - Schematic Diagram - Magnetofluidynamic Vortex Concept

3.2 THE VORTEX AMPLIFIER

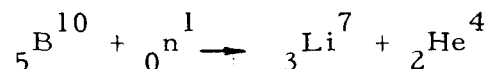
The principles of operation and detailed parametric analysis of the vortex amplifier will be described in detail in Section 5 of this report. A brief description of its operation is provided here to facilitate the understanding of the preliminary studies and selection of the most suitable concept.

The vortex amplifier is a fluid-state control element having no mechanical moving parts. The control is produced by interaction between two fluid flows. The main supply flow enters the device in a direction parallel to the vortex axis and at negligible velocity. The flow passes through a mixing zone in an annular sheet into the main vortex chamber. In the absence of control flow, the main flow proceeds radially inward toward the central outlet of the vortex chamber. In this condition the maximum flow passes through the device.

The control flow enters the mixing region in a direction tangential to the cylindrical wall. The tangential control flow imparts a rotational component to the main supply flow, and the combined flows pass into the vortex chamber with both tangential and radial components. Centrifugal effects create a radial pressure drop. The net result of this pressure drop is to decrease the flow through the outlet orifice. If the control flow and pressure are properly modulated, a desired outlet flow or pressure can be obtained. Depending upon the design, a vortex amplifier can be used to amplify changes in input pressure or flow.

3.3 THE MAGNETOHYDRODYNAMIC SENSOR

As originally visualized, the neutron sensor was to have the basic form of a vortex amplifier. The annular gap through which the gas flows is traversed by a radial magnetic field. The gas on entering the gap flows between rings of conducting material which contains a significant percentage of Boron-10, or other element which has high neutron capture cross-section and emits energetic particles. In the case of Boron-10, the following reaction takes place in a neutron flux:



A portion of the alpha particles emitted go into the annular gap. There they collide with the gas molecules, ionizing some of them. The energy of the nuclear reaction which stays with the rings heats the material. The gas flow helps cool the rings.

At the point where the gas leaves the annular gap, there are rings of metallic material which serve as electrodes. If a fixed electric potential is applied between the emitting rings and the electrodes, current will flow. (The voltage must not be high enough to cause breakdown and discharge through the gas, however.) This current has two components, the alpha particles themselves, and the conduction current due to ionization of the gas in the gap. The magnitude of this current is, of itself, a measure of the neutron flux. However, the purpose of this sensor concept is to provide a pneumatic signal analogous to the neutron flux.

Let us set the gas pressure to put the density in a range where the mean free paths of the alpha particles, electrons and ions are all smaller than the gap dimensions. Then the gas can be regarded as a continuum for fluid dynamic purposes. The current flowing through the gas in the presence of the radial magnetic field will result in a tangential force on the gas. The schematic diagram Figure 3-1 shows the vector relationship between the current density, j , the magnetic flux density, B , and the force per unit volume, F .

This magnetofluidynamic force in the tangential direction tends to swirl the gas, giving it angular momentum, in much the same manner as a control jet in a conventional vortex amplifier. By applying a suitable pickup at the outlet of the sensor, a pneumatic signal which is a function of the neutron flux is derived.

The concept just described was the starting point of the feasibility study reported in this document.

3.4 PRELIMINARY ANALYSIS - MAGNETOFLUIDYNAMIC AND ELECTROFLUIDYNAMIC PRESSURE GENERATORS

The original scope of the investigation included only the crossed field magnetofluidynamic sensor. From Figure 3-1 it may be seen that the proposed device is analogous to a motor with a gaseous conducting armature. Once a realistic model of the conduction and energy exchange processes in the armature annulus has been understood, the almost unavoidable accumulation of ions could be predicted and the advantage of the electrofluidynamic mechanism became apparent. As will be seen, the relative velocities of electrons, ions, and gas are all-important.

To start very simply, if ion-electron pairs are generated in the armature of axial length, L , at a rate dn/dt per unit volume, a steady state will be reached in which the collected current density

$$j = qL \frac{dn}{dt} \quad (3-1)$$

and

$$\frac{dp}{dx} = j \times B \quad (3-2)$$

If the gas is free to move, then within limits of inviscid flow, gas momentum, δv ,

$$\delta v(t) = (j \times B)t \quad (3-3)$$

The maximum velocity at which ions can be removed by the field is $b_i E$, so that once the gas acquires a velocity, the ion current is in the direction of the resultant of $b_i E$ and v_g . Thus, a self-limiting situation is asymptotically approached in which the total net velocity is due to the gas, and E exactly cancels $v_g \times B$. Since the electrons are removed faster (by hundreds to thousands of times) a net positive charge builds up (diffusion controlled in shape and recombination controlled in magnitude) in a thin layer near the ion collector where the majority of the potential drop occurs and a thicker layer near the electron collector where a much smaller drop exists. In the remaining space a very low electric field remains. Losses are taken up mainly by the driving forces in the thin layers. The net circuit current is reduced by diffusion of ions back to the electron collector but the circumferential component $q n_i v_g$ is now much larger than $L (dn/dt)$. The ultimate balance is when net collected current crossed into B balances drag loss around the velocity circuit. At low equilibrium charge densities ($< 10^{10} \text{ cm}^{-3}$), the steady state is achieved very slowly. The governing mechanism in achieving steady state is ion diffusion, an already very slow process, slowed even further by the magnetic induction. A source of instability is wall charging which has been ignored since the primary purpose of this argument is to establish the nature of the approach to steady state.

The mechanism for approach to steady state speeds up with increasing charge and in direct proportion to the rate at which axial flow through the armature is externally introduced. To assume a purging rate of 100 times per second (the required response rate for

the entire sensor is half this) and a circumferential flow velocity of several meters per second is realistic (about one circuit per armature volume). The maximum dn/dt will be (as later shown) about 10^{14} electrons per $\text{cm}^{-3}/\text{sec}$ or 10^{20} per $\text{M}^{-3} \text{ sec}^{-1}$. $j \times B$ is about 0.1 Newton M^{-3} or 1.5×10^{-7} psia for each cm of circumference and cm of axial dimension. The evaluation optimistically ignores the problem of recollecting the ions at such high gas velocities. The field need be large enough that $b_e E \gg v_g$, typical values for b_e being 0.1 to 10 $\text{m}^2 \text{ volt}^{-1} \text{ sec}^{-1}$.

Although it is detrimental to the MFD generation, the excess density of heavy ions in a charged region that results from the low mass of the electron relative to the ion can be used to advantage in the electrofluidynamic generation of pressure gradients. Comparison of the results of the preliminary MFD analysis with prior results on EFD provides a quick measure of the advantage of the EFD pressure generator or (just as accurately) pump.

Stuetzer (1, 2, 3) has analyzed and with others (4, 5, 6) has experimentally verified the EFD pumping mechanism. In the EFD pump, the electrons are collected as efficiently as possible prior to or at the inlet to the pump. The acceleration of the ions in the electric field and loss of their excess momentum to the fluid drags the fluid creating a pressure gradient in the direction of the electric field.

The fundamental equations for the rectilinear configuration (Figure 3-2) are:

$$nq = \rho = \epsilon \frac{dE}{dx} \quad (3-4)$$

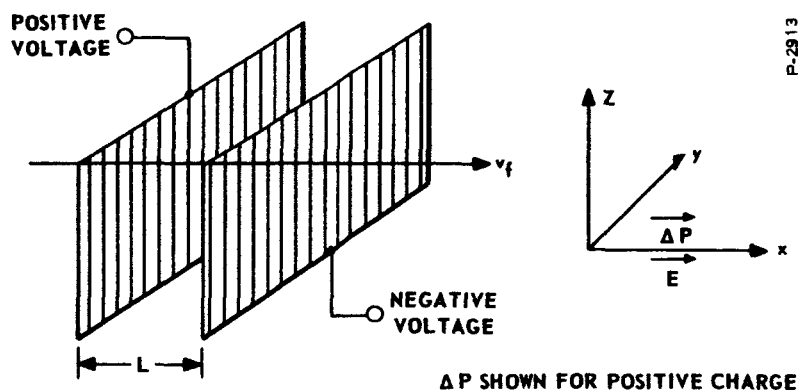


Figure 3-2 - Schematic Configuration of Rectilinear Electrofluidynamic Pressure Generator

where

$$E \text{ is in the } x\text{-direction and } \frac{dE}{dy} = \frac{dE}{dz} = 0$$

and

$$\epsilon = \text{dielectric constant of the fluid}$$

$$j = \rho v \text{ is the current density (in the } x\text{-direction and constant)} \quad (3-5)$$

$$= \rho_0 v_f \text{ where } \rho_0 \text{ is charge density prior to entering the pump field.}$$

$$\rho \frac{dv}{dx} = -v \frac{d\rho}{dx}, v = v_i + v_f, \frac{dv}{dx} = \frac{dv_i}{dx}, \text{ and } v_i = bE \quad (3-6)$$

$$\frac{dp}{dx} = \rho E \quad (3-7)$$

Solutions for ρ , E , and p explicitly in x are given in References 2 and 3, and are:

$$E = \left[\frac{2jx}{\epsilon b} + \left(E_0 + \frac{v_f}{b} \right)^2 \right]^{1/2} = \frac{v_f}{b}, \quad (3-8)$$

where

$$E_0 = \text{field at } j = 0$$

$$\rho = \frac{j}{b} \left[\frac{2jx}{\epsilon b} + \left(E_0 + \frac{v_f}{b} \right)^2 \right]^{-1/2} \quad (3-9)$$

and the pressure differential across a pump of length L

$$p_i = \frac{\epsilon}{2} \left[\frac{2jL}{\epsilon b} - \frac{2v_f}{b} \left(E_0 + \frac{v_f}{b} \right) \left(\sqrt{\frac{2jL}{b} \left(E_0 + \frac{v_f}{b} \right)^{-2} + 1} - 1 \right) \right] \quad (3-10)$$

Implicit in these equations are the assumptions that flow is laminar, that b is constant, that diffusion losses to walls, wall charging, turbulence, and compressibility are negligible, and that the fluid is normally insulating. As Stuetzer and others have shown experimentally (1, 2, 3, 5), these assumptions are valid for liquids. Pressure differentials of several psi can be generated by various configurations with tens of kilovolt sources. The cited work had high pumping efficiency

as a primary objective, and efficiencies of 20 percent were reached for kerosene and freon. Efficiencies of a percent or less are predicted for gases such as SF_6 and air. Measurements on these gases showed⁽¹⁾ that pressures of 0.01 psia at 10^6 VM^{-1} were achieved in a corona ionizer and pump combined. The apparent linearity of pressure output with applied voltage indicates charge densities less than 10^{12} cm^{-3} (10^{18} M^{-3}).

The comparison of 10^{-2} psia produced by EFD pumping of air with the 10^{-6} psia predicted for MFD pumping of H_2 indicated that the EFD pumping had more potential than MFD for the neutron flux sensor. As a result, the feasibility study was redirected toward the more promising EFD concept.

REFERENCES FOR SECTION 3.4

1. O. M. Stuetzer, "Ion Drag Pressure Generation," J. Appl. Phys. 30, 984-994, July 1959.
2. O. M. Stuetzer, "Instability of Certain Electrohydrodynamic Systems," Phys. Fluids 2, 642-648, November - December 1959.
3. O. M. Stuetzer, "Ion Drag Pumps," J. Appl. Phys. 31, 136-146, January 1960.
4. O. M. Stuetzer, "Electrohydrodynamic Components," IRE Trans. on Component Parts, 56-74, June 1961.
5. G. V. Jorgenson and E. Will, "Improved Ion Drag Pump," Rev. Sci. Instr. 33, 55-56, January 1962.
6. O. M. Stuetzer, "Apparent Viscosity of a Charged Fluid," Phys. Fluids 4, 1226-1231, October 1961.
7. O. M. Stuetzer, "Magnetohydrodynamics and Electrohydrodynamics," Phys. Fluids 5, 534-544, May 1962.
8. D. J. Rose, "Mobility of Hydrogen and Deuterium Positive Ions in Their Parent Gases," J. Appl. Phys. 31, 643 (1960).
9. L. B. Loeb, "Basic Processes of Gaseous Electronics," University of California Press, Berkeley and L.A., 1955.
10. E. W. McDaniel, "Collision Phenomena in Ionized Gases," John Wiley and Sons, New York, 1964.

11. H. Etherington, Nuclear Engineering Handbook, McGraw-Hill, New York, 1958, pp. 13-58, 10-131 to 134, 12-151.
12. S. C. Lind, C. J. Hochanadel, and J. A. Ghormley, "The Radiation Chemistry of Gases," Reinhold, New York, 1961, Ch. 7.

SECTION 4

EFD PUMP ANALYSIS

4.1 GENERAL DISCUSSION

The analysis described in Section 3.4 on EFD pumps was primarily related to power efficiency. The basic investigation involves the evaluation of the use of EFD pumping in pressure signal transducers.

The choice of relationships between physical variables which may be used in measurement, and the conditions under which they may be used are dictated by the requirements for sensitivity, repeatability of the sensor's input-output relationship, and the degree to which these are, or can be made, insensitive to the sensor's environment. Where any of these performance characteristics are better than required for any specific application, tradeoffs may be made for reduction of power consumption, weight and size, or to meet other desirable system functions.

The ensuing analysis is aimed at predicting the performance, under conditions of practical application, of an EFD pump generating a pneumatic differential pressure that is uniquely related to ionization of the working fluid. The ionization is proportional to the neutron flux in the range 10^{12} fast neutrons $\text{cm}^{-2} \text{sec}^{-1}$ or less.

The environment is that of a propulsion reactor: temperature varying from 200°R to 800°R ; γ -ray background of $5 \times 10^9 \text{ erg gm}^{-1} \text{ hr}^{-1}$ at full-power and as high as $5 \times 10^7 \text{ erg gm}^{-1} \text{ hr}^{-1}$ at low power for re-start control, and moderate vibration and acceleration under boost launch and propulsion. Hydrogen, stored as liquid, is vaporized for use as the propellant and is available at pressures up to 300 psi.

Within these constraints, the engineering feasibility of the EFD pump can be predicted for neutron flux to pneumatic pressure conversion. The method of neutron to ion conversion and the evaluation leading to the choice of hydrogen for the working fluid are described in this section. The pump performance is analyzed for the particular application including theory, practical configuration, environmental sensitivity, and a description of the experiments that will verify the analytic results.

4.2 THEORETICAL ANALYSIS

4.2.1 Neutron Conversion to Current Density

Except for establishing the upper limit of ion density available in the pump fluid, the means for neutron conversion need not be interrelated with the design of the pump.

Two conversion reactions that have reasonable cross-sections and that produce excess energy in the form of ionizing particles are worth considering. One is the absorption of thermal neutrons by B^{10} with decay to Li^7 and a 1.7 Mev α -particle. The other is the fission of U^{235} on absorption of a neutron. Although the product energies of fission are greater, the larger cross-section of the B^{10} makes its reaction more efficient. This comparison and a discussion of the conversion coating problem is presented in more detail in Section 6.2.4.

The comparison between B^{10} as a constituent in a gaseous compound such as BF_3 and as an elemental wall coating is quickly made by noting that a coating thickness equal to the range of the α -particle product, may contain up to 3 mgm/cm² of elemental boron. About 1/8 of the theoretical α -particle ionizing is done in one α -range in the gas on one side of the coating so that a four-sided chamber would increase the ionization at a given neutron flux by four times. For BF_3 , the mass thickness of elemental boron per α -range is about 1 mgm/cm². The resultant conversion ratios of ionization density to neutron flux are about the same.

The coating presents a much simpler problem in that, with it, any gas may be used along with suitable chamber dimensions, e.g., honeycomb sections of mesh size equal to the α -range for the gas at the working pressure. Also, the quantity of enriched boron necessary is considerably less -- even for a sensor that recycles the gas. Further, the sensitive volume is controlled by the coating so that the response time for equilibrium ionization is only the chamber length divided by the gas velocity. In the following section, consideration of the requirements on the working fluid will add to the advantages of a coated chamber over a BF_3 working fluid.

The conversion rate from an isotropic flux of neutrons to alpha particles is:

$$\phi_{\alpha} = \frac{R_B \times Q_B}{M_B} \phi_{o_n}$$

where the subscript "B" here denotes Boron.

Approximately one-eighth the total ionization from ϕ_α will be in the gas. Each alpha particle produces about 5×10^4 ions and is totally absorbed in a range of 3.6 mm or less of the gas at ten atmospheres and 460°R.

To minimize the ionization loss as the range increases with decreasing density (increasing temperature at constant pressure), the chamber diameter should be four times the minimum range, i.e., 1.0 cm. The wall area then is $\pi \text{ cm}^2$ per cm axial length and the cross-sectional area is $\pi/4$. The average ion current density then is

$$j = \frac{5 \times 10^4}{\pi/4} \times \frac{\pi}{8} q \phi_\alpha$$

The boron will be about 2 milligram cm^{-2} thick. At an enrichment of 0.75 B¹⁰, $j = 1.6 \times 10^{-11} \phi_{\text{on}}$ amp M^{-2} (where ϕ_{on} is neutrons/ cm^2 - sec).

4.2.2 The Working Fluid

The conduction processes in cool weakly ionized gases are not complicated by the strong nonlinear inductive interactions of the high charge densities and currents of plasmas. However, the normally assumed constant conduction parameter, ion mobility, is generally not constant at values of electric field beneath those that will sustain a discharge. Also, the mobility and the recombination coefficient are both extremely sensitive to molecular type. These phenomena are extensively treated in the first six chapters of Reference 9. Being relatively low energy interactions, they are also, as a rule, extremely sensitive to temperature.

The implication of these complexities to the EFD transducer design is that long-term stability will be achieved most quickly by working with a gas of extreme purity and, if possible, one having a simple atomic and molecular structure. The latter is merely another way of saying that the numbers of available energy and charge states should be low and their excitation energies should be high so that temperature effects are minimized. It also minimizes radiative energy exchange, thereby increasing the discharge-sustaining potential drop.

The overriding need is for purity, since the advantage of structural simplicity of the molecule is lost if as little as 1 ppm of a strongly electron attaching species is present. One qualification which

must be met by the working fluid in an EFD transducer is that it must be available at the time required free of molecular or atomic oxygen to better than one part in ten million. (This is a much simpler specification to meet than a tolerance of this order of magnitude on a mixture.) Only helium and hydrogen can meet the requirements, and hydrogen is already available in great supply aboard the vehicle on which the sensor will be used.

The required freedom of O and O₂ is expected from propellant grade hydrogen because the radiation field will establish an equilibrium between H₂O, O, O₂, and OH. The water molecule does not attach electrons and since it will predominate by at least an order of magnitude over the rest, the concentration of electron attaching molecules will be reduced well below the two ppm of O₂ (half free, half in CO₂) specified for propellant hydrogen (Reference Mil-P-27201A, 1 September 1964).

Although values of rate constants are unknown, an estimate of the active oxygen available in propellant hydrogen while under irradiation can be made. The situation is dominated by three conditions:

- (1) The stability of H₂
- (2) The stability of the H₂O molecule
- (3) The low absolute molecular concentration of O₂
(maximum possible is 2×10^{-6} O₂ to H₂)

A review of experimental knowledge of the oxidation of H₂ and the decomposition of water by radiation in References 11 and 12 leads to the conclusion that O₂ and oxygen radicals will be present at much lower concentrations by at least two orders of magnitude than H₂O which itself does not attach electrons.

The basic problem with gaseous impurities in any gas is the extreme sensitivity of the ion and electron mobilities and recombination coefficients to electron attaching impurities. Ion mobility appears directly in the transfer functions of the sensor while a variation of the recombination rate would change the ionization density for a particular neutron flux at high ionization densities.

The availability of large quantities of hydrogen permits sensor inside walls to be ignored as sources of contamination since high purging rates may be used during sensor operation.

Although ion mobilities have been measured only at much higher ratios of electric field to gas pressure than assumed for reliable transducer operation, there is reason to suspect impurity effects to be worse as the ion drift velocities decrease.

Extrapolating the data that is available for ion mobilities in hydrogen (Reference 8) leads to the estimate that it lies between a condition of holding constant and one of varying as the first power of the electric field, i.e., the mobility.

$$b = \beta E^n$$

where there is some uncertainty in β and n . The lowest few experimental points of Rose and Clark lie on a line

$$b = 5 \times 10^{-10} \frac{E}{p} \frac{M^3 \text{ Atmos}^2}{\text{Volt}^2 \text{ sec}}$$

For the purposes of feasibility prediction, very low ratios of electric field to pressure have been assumed. The reason for the assumption is that intermittent discharging, arcing, or sparking cannot be permitted except at very low frequency of occurrence and with recovery times less than the required response time of the sensor.

Arcs and sparks result when strings of dense charge are formed in the direction of the electric field. Having high conductivity, they both short part of the electrode gap and appear as sharp field termini or mobile corona points. They propagate across the gap, and if sufficient power is available, maintain themselves as conductive channels. Such strings can be caused by massive high energy fission products, events involving primary cosmic particles, or even by random spatial and temporal peaks in the ionization involved in the measurement. Currents of a hundred milliamperes or larger are necessary to sustain an arc.

The normal glow discharge is not expected at pressures of 10 atmospheres. However, the photoemission from electron-molecule collisions in the anode-cathode drop regions can excite photoelectrons from the cathode. It is an experimental fact that a minimum anode-cathode fall is necessary to sustain the normal discharge. For hydrogen, 170 to 230 volts (depending on cathode material) is necessary.

Caution then dictates maximum cathode-anode voltages of 200 volts and quick recovery power supplies limited to one milli-ampere or less. Electric field strengths of 10^5 V M^{-1} in pumps built

of relatively open (95 percent) grids separated by two millimeters in the direction of gas flow provide a practical structure. The configuration has dimensional flexibility, approximates closely a rectilinear configuration, adjusts simply to avoid sustained discharges, permits neglect of wall charging as a problem source, and so provides a model for analysis as well as a model for experimental verification of the analysis.

4.2.3 Theory of the Gaseous EFD Hydrogen Pump

The preliminary analysis in Section 3.3 cited the results of previous work (Reference 1-7) on EFD pumps to compare EFD with MFD as transducer mechanisms. The cited work was based on constant ion mobility, that is, the ion drift velocity is linearly dependent on the electric field intensity. As already discussed, hydrogen, about which more is known than any except the rare gases, appears to exhibit at low fields and high pressures a first power dependence of mobility on electric field intensity. At the very low values of E/p assumed here, the mobility very likely lies between being constant and having the first power dependence, as discussed previously. (A persistent dependence greater than first power would result in a zero mobility at appreciable field strengths.)

The following analysis is idealized to the extent that it is assumed:

- (1) Electrons are completely collected at the pump inlet electrode.
- (2) Recombination times are large compared to the time gas spends in the pump.
- (3) Diffusion losses of ions inside the pump are negligible, or if not negligible, small, and the variations in them due to temperature changes are negligible.

These assumptions are justified in Section 4.2.4 after the reader is familiar with the dimension, geometry, and character of the proposed pump.

A solvable set of differential equations results if the further assumption is made that the variation in fluid velocity is negligible. The resulting set of differential equations can be solved if the divergence of the fluid velocity is assumed negligible relative to the divergence of the ion velocity. The attainable EFD pressure gradients are small enough relative to the mean pressure that this assumption is justified.

The governing equations are:

$$nq = \rho = \epsilon \frac{dE}{dx} \quad (4-1)$$

$$j = \rho v = \rho_o v_f \quad (4-2)$$

$$\rho \frac{dv}{dx} = -v \frac{d\rho}{dx} \approx \frac{d(bE)}{dx} \quad (4-3)$$

$$\frac{dp}{dx} = \rho E \quad (4-4)$$

$$b = \beta E; \text{ i.e., } b \text{ is not a constant} \quad (4-5)$$

A new set of differential equations results under the same conditions and assumptions (except on b) as before. Dropping the approximation sign in equation (4-3), and substituting from equation (4-2) for v, and from equation (4-1) for dE/dx.

$$- \frac{j}{\rho} \frac{d\rho}{dx} = 2 \beta \rho E \frac{dE}{dx} = \frac{2\beta}{\epsilon} \rho^2 E \quad (4-6)$$

and differentiating

$$\frac{d^2 \rho}{dx^2} - \frac{3}{\rho} \left(\frac{d\rho}{dx} \right)^2 = \frac{-2\beta}{j\epsilon} \rho^4 \quad (4-7)$$

Alternatively, substituting from equation (4-1) for ρ in equation (4-6)

$$\frac{d^2 E}{dx^2} = \frac{2\beta\epsilon}{j} E \left(\frac{dE}{dx} \right)^3 \quad (4-8)$$

and combining equations (4-6) and (4-4)⁴

$$\frac{dp}{dx} = \frac{-\epsilon j}{2\beta\rho^2} \frac{d\rho}{dx} \quad (4-9)$$

The solutions are:

$$\rho = \left[\frac{3}{\epsilon} \sqrt{\frac{\beta}{j}} \left(\frac{\epsilon}{3} \sqrt{\frac{j}{\beta}} \rho_o^{-\frac{3}{2}} + x \right) \right]^{-2/3} \quad (4-10)$$

$$p_i = \frac{3}{2} \left(\frac{\epsilon}{3} \right)^{\frac{1}{3}} \left(\frac{j}{\beta} \right)^{\frac{2}{3}} \left[\left(\frac{\epsilon}{3} \sqrt{\frac{j}{\beta}} \rho_o^{-\frac{3}{2}} + x \right)^{\frac{2}{3}} - \left(\frac{\epsilon}{3} \sqrt{\frac{j}{\beta}} \right)^{\frac{2}{3}} \rho_o \right] \quad (4-11)$$

$$E = \left[\frac{3j}{\epsilon\beta} \left(x + \frac{\beta\epsilon}{3j} E_o^2 \right) \right]^{\frac{1}{3}} \quad (4-12)$$

Examination of equation (4-11) shows that:

$$p_i = \left(\sqrt{\frac{\epsilon}{3}} \frac{j}{\beta} \right)^{\frac{2}{3}} x \text{ for } j < 10^{-3} \text{ amp } M^{-2}$$

$$p_i = \frac{3}{2} \left(\sqrt{\frac{\epsilon}{3}} \frac{j}{\beta} x \right)^{\frac{2}{3}} \text{ for } j > 0.1 \text{ amp } M^{-2}$$

Substitution of the values:

$$\epsilon = \epsilon_o = 8.6 \times 10^{-12} \text{ FM}^{-1}$$

$$j = 16 \text{ amp } M^{-2} \text{ (at } \phi_n = 10^{12} \text{ cm}^{-2} \text{ sec}^{-1} \text{)}$$

$$\beta = 5 \times 10^{-12} \text{ (for } H_2 \text{ at 10 atmos. pressure)}$$

$$x = 0.01 M$$

yields,

$$p_i = 0.31 \text{ psia}$$

Comparison with the results of Section 3.4 indicates that the current to pressure conversion will be between the half-power (x may vary inversely as the square root of n_i at very high change densities) and the two-thirds power of the pump current, depending on the actual behavior of the hydrogen ion mobility at low E/p .

Using the 2/3 power of current relationship, and 10^{-5} psia as the smallest useful output, 2.8×10^{-5} amp M^{-2} will be the least detectable current. The maximum current (at a neutron flux of 10^{12} $\text{cm}^{-2} \text{ sec}^{-1}$) is 16 amp M^{-2} . The relative range then will be 5.7×10^5 , and the minimum detectable neutron flux -- $1.75 \times 10^6 \text{ } n \text{ cm}^{-2} \text{ sec}^{-1}$.

4.2.4 The Effects of Recombination, Diffusion, and Space Charge

In the idealized analysis, the charge losses to diffusion and recombination processes were ignored. Also, the reduction of effective pump chamber length by the intrusion into it of the virtual space charge limited anode was ignored.

One basis for the first two of these idealizations lies in the times required for these mechanisms to become effective. According to McDaniel (Reference 10, p. 557), the relaxation from an initial electron energy in H₂ at 10 atmospheres pressure will proceed with a characteristic time of 0.1 millisecond. Assuming an average energy following generation in the order of 10 ev, it will take new electrons 0.4 millisecond to reach energy of 0.2 ev -- still a quite "hot" electron. At the maximum ion density ($2.5 \times 10^{13} \text{ cm}^{-3}$), the shielding length of 8 ev electrons will be about 10 percent of the separation of the electron collecting ribbons.

At the lowest possible gas velocity anticipated, 5 M/sec, the average electron will still be at an effective temperature of several hundred degrees C and will not be in the region of rapid recombination when it enters the electron collector in the pump. The worst conditions will be at the highest charge concentration and lowest temperature -- mutually exclusive conditions. Of course, a fraction of electrons will spend additional time in the chamber until they migrate back out to the anode or do recombine.

Recombination in the most pessimistic view is effective only at high flux where sensitivity is no problem. Assuming the worst case possible, the recombination rate a , is $2.5 \times 10^{-8} \text{ cm}^3 \text{ sec}^{-1}$ at a numerical charge density, n , of 10^{12} cm^{-3} . At the highest flux, the ion pair production, r , is $5 \times 10^{14} \text{ cm}^{-3} \text{ sec}^{-1}$.

The equilibrium charge density, if the gas were not flowing, would be at,

$$\begin{aligned}\frac{dn}{dt} &= -a n^2 + r = 0 & (4-13) \\ n^2 &= \frac{r}{a} = \frac{5 \times 10^{14}}{2.5 \times 10^{-8}} = 2 \times 10^{22} \\ n &= 1.5 \times 10^{11}\end{aligned}$$

If there were no recombination and the charge density were reduced only by the gas velocity of $5M \text{ sec}^{-1}$, n would be 10^{12} cm^{-3} . At one order of magnitude down in flux ($10^{11} \text{ neutrons cm}^{-3} \text{ sec}^{-1}$), the two effects are about equal, and below 10^{10} cm^{-3} the recombination is negligible relative to the gas flow in determining the charge density.

If experiment discovers a total saturation (definitely not expected), the top decade can be covered by including a less sensitive uncompensated internally converting neutron pump physically located in series with the sensitive wide range compensated pumps. The high-range pump would be switched on at an experimentally determined point at which the measurement is beginning to be disturbed by recombination. Ions would then be pumped within 0.5 millisecond after formation.

Since the gas never takes more than 2 milliseconds to get through the neutron chamber and pump, ion loss by diffusion will be negligible. In a millisecond, diffusion will produce an rms displacement of an ion of about 10^{-2} cm .

In the idealized analysis of Section 3.2.3, no account was taken of the shielding of the inlet of the pump chamber by the positive space charge sheath at the ion collector. This effect appears in the top three decades. However, since in any case the same amount of work is done on the ions, the difference will be in the efficiency with which this work is transferred to the fluid. The sheath is a small fraction of the chamber length in the upper two decades. It might be expected that the ratio of field strength to pressure is then high enough that constant ion mobility prevails. The first power response (equation (2-19)) would then rule the pressure-current relation. If so, a saturation effect would be welcome since it would help to achieve the desired logarithmic output.

In summary, the analysis of Section 3.2.3 applies at low charge density. At high charge density, the effects discussed are applicable. However, until their nature and where they occur are empirically determined, it may be assumed that in the worst event two pumps operating at different neutron flux conversion efficiencies can cover the entire range that is predicted for the ideal pump. For example, at high fluxes the neutron conversion chamber may be operated by itself as a low efficiency single section pump.

REFERENCES

1. O. M. Stuetzer, "Ion Drag Pressure Generation," J. Appl. Phys. **30**, 984-994, July 1959.
2. O. M. Stuetzer, "Instability of Certain Electrohydrodynamic Systems," Phys. Fluids **2**, 642-648, November - December 1959.
3. O. M. Stuetzer, "Ion Drag Pumps," J. Appl. Phys. **31**, 136-146, January 1960.
4. O. M. Stuetzer, "Electrohydrodynamic Components," IRE Trans. on Component Parts, 56-74, June 1961.
5. G. V. Jorgenson and E. Will, "Improved Ion Drag Pump," Rev. Sci. Instr. **33**, 55-56, January 1962.
6. O. M. Stuetzer, "Apparent Viscosity of a Charged Fluid," Phys. Fluids **4**, 1226-1231, October 1961.
7. O. M. Stuetzer, "Magnetohydrodynamics and Electrohydrodynamics," Phys. Fluids **5**, 534-544, May 1962.
8. D. J. Rose, "Mobility of Hydrogen and Deuterium Positive Ions in Their Parent Gases," J. Appl. Phys. **31**, 643 (1960).
9. L. B. Loeb, "Basic Processes of Gaseous Electronics," University of California Press, Berkeley and L.A., 1955.
10. E. W. McDaniel, "Collision Phenomena in Ionized Gases," John Wiley and Sons, New York, 1964.
11. H. Etherington, Nuclear Engineering Handbook, McGraw-Hill New York, New York, 1958, pp. 13-58, 10-131 to 134, 12-151.
12. S. C. Lind, C. J. Hochanadel, and J. A. Ghormley, "The Radiation Chemistry of Gases," Reinhold, New York, 1961, Ch. 7.

SECTION 5

VORTEX AMPLIFIER ANALYSIS

5.1 BASIC PRINCIPLES OF VORTEX AMPLIFIERS

This section gives a detailed analysis of vortex amplifiers as related to the specific application of the neutron sensor. The results of this section, together with the results of Section 4, are combined in Section 6 to give an overall description of the complete neutron sensor system.

5.1.1 Description of Vortex Amplifier

The vortex amplifier is a fluid state control element having no mechanical moving parts. The control effect is produced by the pressure drop across a vortex flow field created by injecting fluid tangentially at the outer wall of a cylindrical chamber. Depending upon the specific design and the manner in which the vortex device is operated, either a pressure amplification or a flow amplification may be obtained.

Figure 5-1 is the schematic of a typical vortex amplifier. The figure also defines the notation for the geometry of the vortex amplifier.

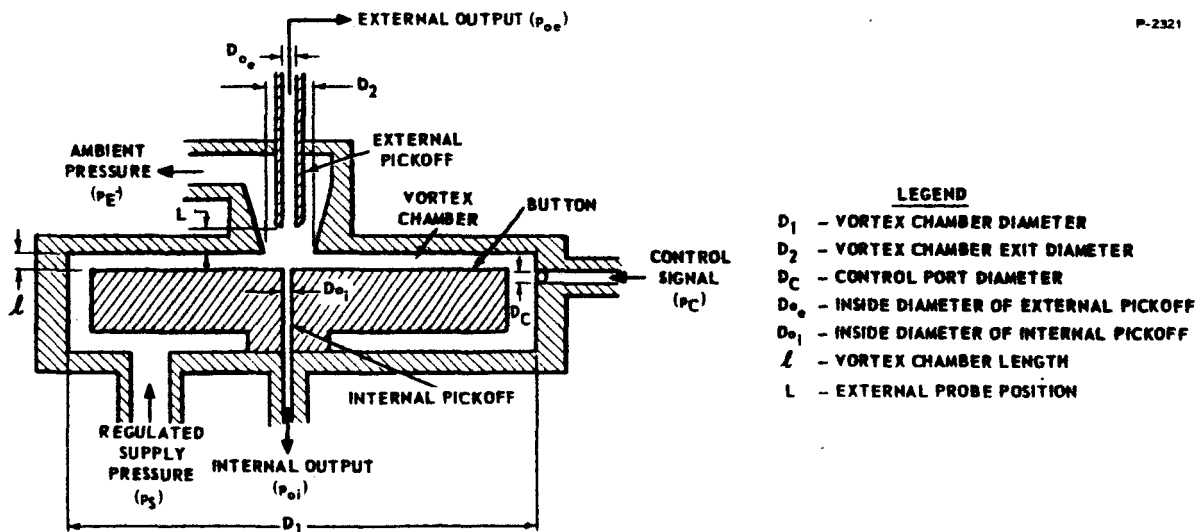


Figure 5-1 - Vortex Amplifier Schematic

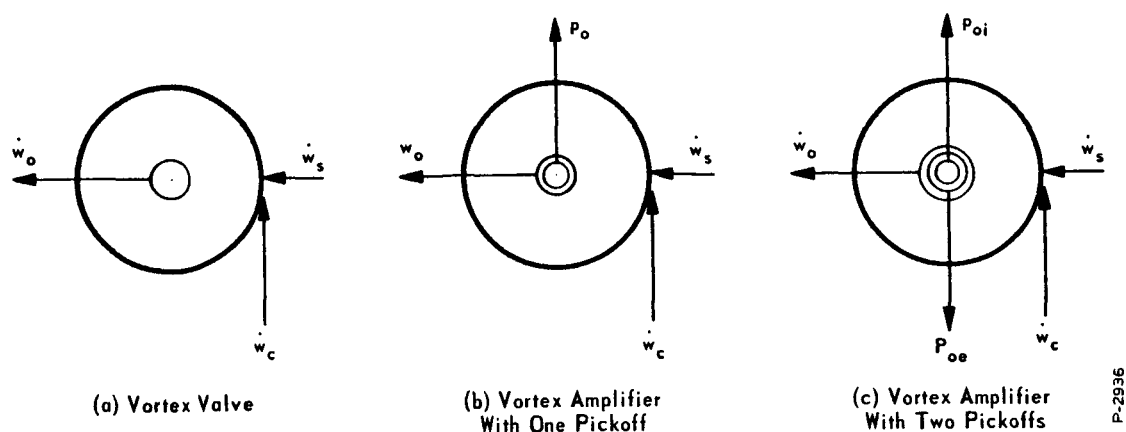


Figure 5-2 - Conventional Representation of Vortex Amplifiers

The main supply flow enters the mixing zone behind the button at low velocity. The flow passes around the button in an annular sheet into the main vortex chamber. In the absence of control flow, the main flow proceeds radially inward toward the central outlet of the vortex chamber. In this condition, the maximum flow passes through the central outlet. When a tangential control flow is provided, a rotational component is imparted to the main supply flow, and the combined flows pass into the vortex chamber with both tangential and radial components. Centrifugal effects create a radial pressure drop which produces a useful change in pressure or flow.

Figure 5-2 shows the conventional representation of vortex devices which will be used for schematics of vortex amplifier systems in this report. Figure 5-2(a) shows a vortex valve which has an outlet orifice but no pressure pickoffs. Figure 5-2(b) shows a vortex pressure amplifier with one pickoff, which could be in either the internal or external position as indicated in Figure 5-1. Figure 5-2(c) shows a vortex pressure amplifier with two pressure pickoffs such as a device with both internal and external pickoffs. Other arrangements are possible. For example, the outlet flow can be taken through a central hole and the pressure output sensed through an outer hole.

5.1.2 Calculation of the Pressure Drop Across a Vortex in an Inviscid Ideal Gas

The control flow is introduced into a vortex amplifier tangential to the circle of diameter D_1 . The control flow mixes with

the supply flow and establishes a tangential velocity component in the vortex chamber. If conservation of momentum can be assumed, the tangential velocity at the outer wall is given by:

$$v_w = \frac{\dot{w}_c v_c}{\dot{w}_s + \dot{w}_c} \quad (5-1)$$

where

v_w = tangential velocity component at outer radius
of vortex - fps

v_c = control velocity - fps

\dot{w}_s = supply flow - lb/sec

\dot{w}_c = control flow - lb/sec

The assumption of perfect momentum exchange is probably not accurate. However, the assumption is satisfactory for the present analysis since it permits the derivation of an equation which can be used to predict the general trends of vortex amplifier performance and the functional relationships among the variables.

The tangential velocity component, v_w , establishes a vortex flow field in the vortex chamber. At any radius in a vortex, the angular rotation is given by:

$$\omega = \frac{v_T}{r} \quad (5-2)$$

where

v_T = tangential velocity - fps

ω = angular velocity - rad/sec

r = radius - in.

The relationship between v_T and r at any two radial positions in a vortex can be described by:

$$\frac{v_{T2}}{v_{T1}} = \left(\frac{r_2}{r_1} \right)^{n-1} \quad (5-3)$$

where

v_{T2} = tangential velocity at radius r_2 - fps

v_{T1} = tangential velocity at radius r_1 - fps

and

$n = 0$ corresponds to a free vortex
($v_T r = \text{constant}$)

$n = 1$ corresponds to a constant tangential velocity
($v_T = \text{constant}$)

$n = 2$ corresponds to a forced vortex
($\omega = \text{constant}$)

In a conventional vortex amplifier, when $v_w = 0$, the pressure drop across the amplifier is essentially that resulting from the flow through the outlet orifice. Therefore, when $v_w \neq 0$, the change in pressure in the radial direction of the vortex field for an inviscid fluid as defined by the radial momentum equation, is approximately:

$$dp = 144 \rho v_T^2 \frac{dr}{r} \quad (5-4)$$

where

p = pressure - psia

ρ = mass density - lb-sec²/in⁴

If the fluid is a perfect gas:

$$\rho = \frac{p}{g R T} \quad (5-5)$$

where

g = standard gravitational acceleration = 386 in/sec²

R = ideal gas constant - lb_m in/lb_f °R

T = absolute temperature - °R

Equations (5-3), (5-4), and (5-5) can be combined and integrated to obtain the change in pressure from an outer to an inner radius. With the restrictions of constant T, and n constant and $\neq 0$, the integrated equation is:

$$\text{Ln} \left(\frac{p_w}{p_i} \right) = \left(\frac{144 v_w^2}{g R T} \right) \left(\frac{1}{2n - 2} \right) \left[1 - \left(\frac{r_i}{r_w} \right)^{2n - 2} \right] \quad (5-6)$$

The primary significance of this equation is the indication that the true input to a vortex amplifier is the tangential velocity at the outer wall, v_w . The value of v_w is changed by varying the momentum of the control flow injected tangentially at the outer wall of the vortex chamber. The control flow momentum is equal to $\dot{w}_c v_c / g$. If perfect momentum exchange between the supply and control flows could be achieved, the value of v_w would be given by equation (5-1).

If the control ports of a vortex amplifier are large, small changes in the control pressure, p_c , produce a given control momentum change, and the device is a pressure amplifier. On the other hand, if the control ports are small, small changes in control flow produce a given control momentum change and the device is a flow amplifier.

A precise correlation between equation (5-6) and the actual performance of a vortex amplifier is difficult. In a real vortex device, the flow is three-dimensional and is influenced by real gas effects. The parameter, n, thus appears to be not an integer and variable and the ratio r_i/r_w is not exactly defined by the physical geometry of the amplifier. However, the equation is useful in that it gives an insight into the nature of the operation of a vortex amplifier.

5.1.3 Actual Vortex Amplifier Performance

Figures 5-3 and 5-4 show plots of v_w versus $p_{oi}/p_{oi \text{ max}}$ for vortex amplifiers having diameters of 1, 2, and 3 in. The data for both of these figures was taken at 30 psig supply pressure with room temperature air. The values of $p_{oi \text{ max}}$ for these curves are 44.7 psia for the 1-in. amplifier with blocked output, 44.3 psia for the 3-in. amplifier, 44.0 psia for the 2-in. amplifier, and 39.2 psia for the 1-in. amplifier with flowing output. Values of v_w were computed from equation (5-1) assuming that:

$$v_c = \frac{1}{12} \sqrt{\left[\left(\frac{2 k g R T}{k - 1} \right) \left[1 - \left(\frac{p_s}{p_c} \right)^{(k - 1)/k} \right] \right]} \quad (5-7)$$

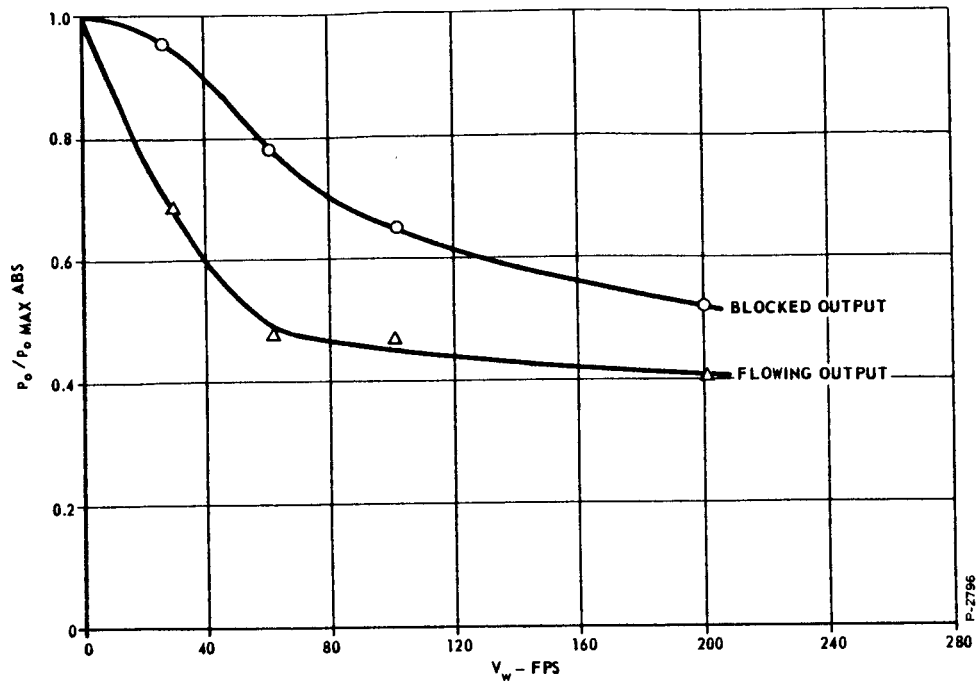


Figure 5-3 - Output Performance of a One Inch Vortex Amplifier

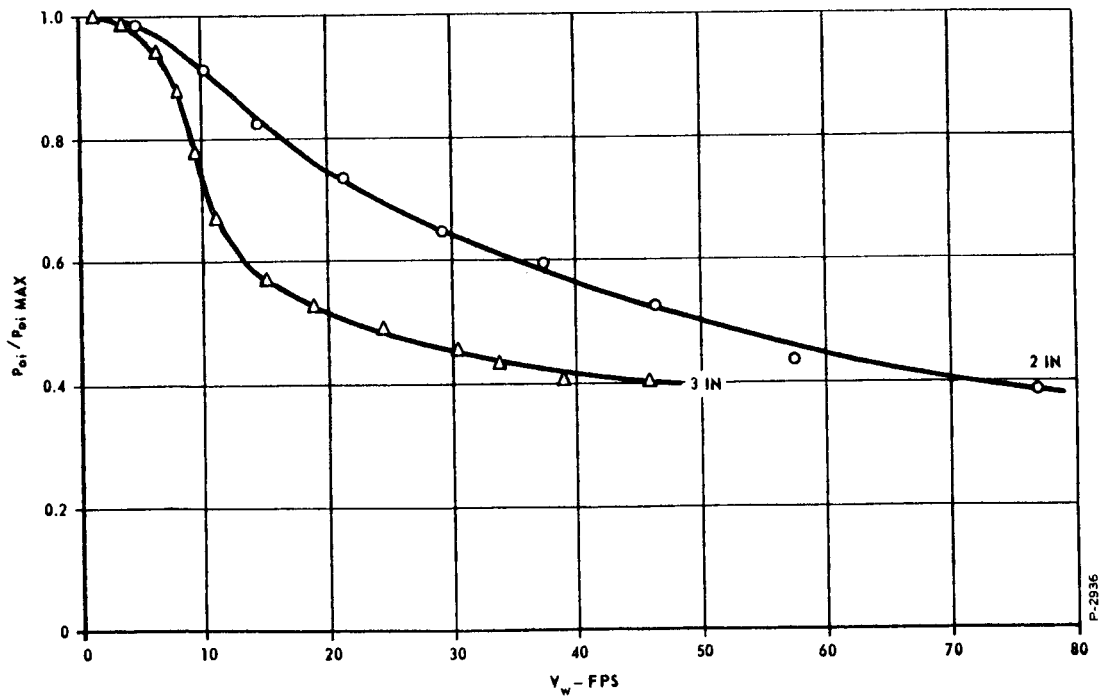


Figure 5-4 - Typical Performance of Two and Three Inch Vortex Amplifiers with Internal Pickoffs at 30 Psig Supply Pressure

for $p_s/p_c < 0.999$ and

$$v_c = \frac{1}{12} \sqrt{\frac{2 g R T}{p_s} (p_c - p_s)} \quad (5-8)$$

for $1.0 > p_s/p_c > 0.999$

where

k = ratio of specific heats - dimensionless

p_c = control pressure - psia

p_s = supply pressure - psia

The significant geometrical parameters of these vortex amplifiers are tabulated in Table 5-1.

Table 5-1 - Vortex Amplifier Parameters

D_1	D_2	D_{oi}	l	D_2/D_1	D_{oi}/D_1	D_{oi}/D_2	l/D_1	l/D_2
inch	inch	inch	inch					
1.0	0.05	0.02	0.070	0.05	0.020	0.40	0.070	1.4
2.0	0.21	0.05	0.125	0.10	0.025	0.24	0.062	0.6
3.0	0.09	0.02	0.109	0.03	0.0067	0.22	0.036	1.2

The curves given in Figures 5-3 and 5-4 indicate that for the specific vortex amplifiers under consideration, the output pressure becomes more sensitive to changes in tangential velocity at the wall as the vortex chamber diameter D_1 increases. A number of factors may account for this effect.

As indicated by equation (5-6), the pressure ratio across an ideal, inviscid, vortex will be most sensitive to changes in tangential velocity when the ratio r_i/r_w is the smallest. Equation (5-6) will give an adequate description of pressures inside the vortex chamber from the outer wall diameter D_1 to the edge of the outlet hole D_2 . At diametrical coordinates less than D_2 , the flow will be three-dimensional and will no longer be described by equation (5-6). Hence, there will be

no exact correspondence between the physical geometry of the vortex amplifier and a r_i/r_w ratio for the vortex flow field. However, there will be a relation between an effective r_i/r_w ratio and the ratios D_{oi}/D_1 and D_2/D_1 . It will be expected that, all other factors being equal, the vortex amplifier having the smallest ratios, D_{oi}/D_1 , and D_2/D_1 , will have the highest gain, $\Delta p_{oi}/\Delta v_w$. Since the form of the three-dimensional flow field will also influence the gain, the relationship between D_{oi}/D_1 and D_2/D_1 , which may be described by the ratio D_{oi}/D_2 , will also be of significance.

In general, Bendix vortex pressure amplifiers have been built with the vortex chamber length, l , at least equal to the diameter of the outlet, D_2 . This is done to insure that in the no-swirl condition the radial pressure drop in the chamber will be insignificant. Deviations from this rule are made in special cases, as for example, when it is desired to obtain good dynamic response. However, experience has shown that too extreme a reduction in l will cause a deterioration in vortex amplifier performance.

Other factors which will effect the performance of vortex amplifiers include Reynolds number and other real gas effects, geometrical imperfections in the individual amplifier, and the efficiency with which the control momentum is transferred to the total flow in a particular unit. There will be a tendency for these factors to be more significant in a smaller unit than a larger.

The greater change in output pressure for a given change in v_w which was obtained with the 3-in. vortex amplifier compared with the 2-in. vortex amplifier is attributed primarily to the smaller diameter ratios D_2/D_1 and D_{oi}/D_1 which are associated with the larger unit. However, the relatively small value of l for the 2-in. unit would also contribute to the difference in gains. The greater value of $\Delta p_o/\Delta v_w$ associated with the 2-in. unit compared with the 1-in. unit is attributed to a greater efficiency of the larger unit. However, the larger value of D_{oi}/D_2 associated with the smaller unit might also be of significance.

From Figure 5-4, the maximum gain of the 3-in. amplifier is 2.8 psi/fps at $v_w \approx 9$ fps. A similar test with a supply pressure of 60 psig gave a gain of 3.8 psi/fps at v_w of approximately 7 fps. These gains are all based on the use of the internal pickoff. Higher gains are possible with the use of a carefully constructed external pickoff.

Figure 5-5 shows the pressure amplification characteristics of the 3-in. diameter amplifier of Figure 5-4 operated at various supply pressures. The maximum pressure gain, $K_p = \Delta p_{oi} / \Delta(p_c - p_s)$, for this particular test is 3600. Tests of similar units have shown higher gains. In order to obtain these high values of K_p , relatively large control ports must be used. As a result, control flow increases rapidly and soon equals the flow from the outlet orifice. At this point, a further decrease in output pressure is impossible unless there is a means of dumping excess control flow. In the test producing the data shown in Figure 5-5, the excess control flow was removed by allowing it to flow backwards through the supply line and vent through the supply pressure regulator. Figure 5-6 shows the control flow, \dot{w}_c , and the outlet orifice flow, \dot{w}_o , as a function of $p_c - p_s$. The data shown in Figures 5-5 and 5-6 is typical of high gain vortex pressure amplifiers. The actual curve will be affected by the working fluid, temperature levels, and the pressure levels and ratios imposed on the device.

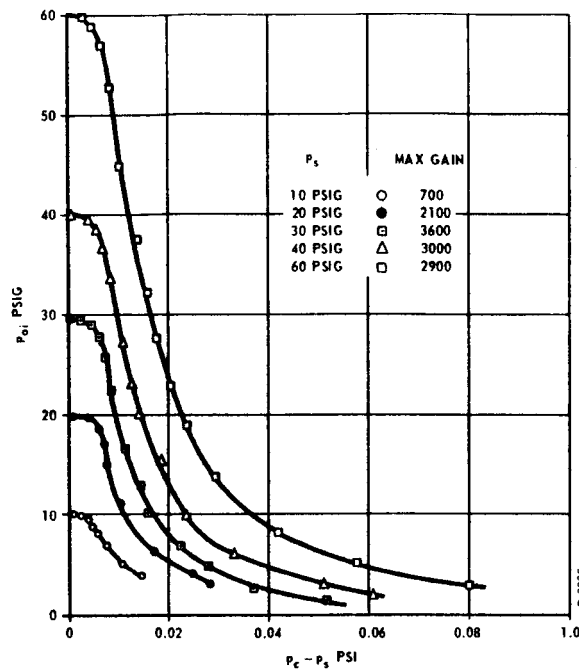


Figure 5-5 - Effect of Supply Pressure on Vortex Pressure Amplifier Performance

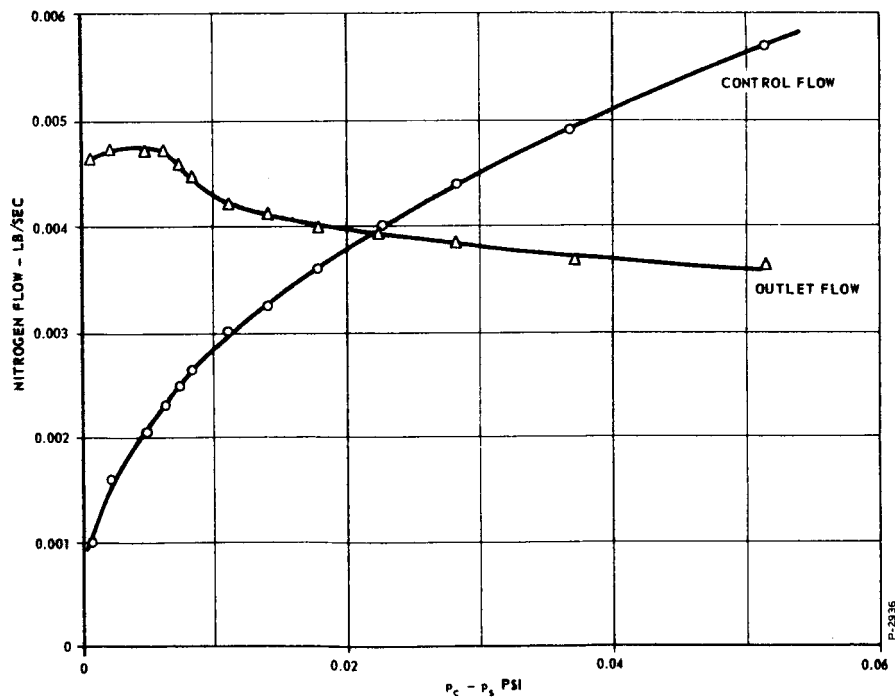


Figure 5-6 - Flows through Three Inch High Gain Pressure Amplifier at 30 Psig Supply Pressure

5.2 FACTORS AFFECTING VORTEX AMPLIFIER PRESSURE GAINS AND OUTPUTS

5.2.1 Temperature Sensitivity

It can be shown from equation (5-6) that the pressure ratio across an ideal vortex amplifier should be independent of the molecular weight and the temperature of the working fluid. The demonstration is as follows:

The flow through the outlet orifice (diameter D_2) is

$$\dot{w}_o = \dot{w}_c + \dot{w}_s = \frac{C_{do} A_2 f_2 (P_u/P_e)}{\sqrt{RT}} \quad (5-9)$$

where

$$f_2 (p_u/p_e) = p_u \sqrt{\frac{2 k g}{(k-1)} \left(\frac{p_e}{p_u}\right)^{2/k} \left[1 - \left(\frac{p_e}{p_u}\right)^{(k-1)/k}\right]}$$

if the flow is subsonic and

$$f_2 (p_u/p_e) = p_u \sqrt{g k} \left(\frac{2}{k+1}\right)^{\frac{(k+1)}{2(k-1)}}$$

if the flow is sonic

where

C_{do} = discharge coefficient of outlet orifice - dimensionless

A_2 = area of outlet orifice - in²

p_u = pressure determining flow through outlet orifice - psia

p_e = vortex amplifier exhaust pressure - psia

Also

$$\dot{w}_c = \frac{C_{dc} A_c f_2 (p_s/p_c)}{\sqrt{RT}} \quad (5-10)$$

where

C_{dc} = control port discharge coefficient - dimensionless

A_c = control port area - in²

Furthermore

$$v_c = RT f_1 (p_s/p_c) \quad (5-11)$$

where

$$f_1 = \frac{1}{12} \sqrt{\frac{2 k g}{(k-1)}} \left[1 - \left(\frac{p_s}{p_c} \right)^{(k-1)/k} \right]$$

since control flow will invariably be subsonic for a pressure amplifier. Substitution of equations (5-9), (5-10), and (5-11) into equation (5-1) gives:

$$v_w = \frac{C_{dc} A_c f_1 (p_s/p_c) f_2 (p_s/p_c) \sqrt{RT}}{12 C_{do} A_2 f_2 (p_u/p_e)} \quad (5-12)$$

Substituting equation (5-12) into equation (5-6) gives:

$$\begin{aligned} \ln \left(\frac{p_w}{p_i} \right) = & \left(\frac{1}{g} \right) \left[\frac{C_{dc} A_c f_1 (p_s/p_c) f_2 (p_s/p_c)}{C_{do} A_2 f_2 (p_u/p_e)} \right]^2 \left(\frac{1}{2n-2} \right) \dots \\ & \left[1 - \left(\frac{r_i}{r_w} \right)^{2n-2} \right] \end{aligned} \quad (5-13)$$

and the pressure ratio across an ideal vortex amplifier operating with an inviscid fluid is independent of temperature and molecular weight.

However, if actual vortex amplifier performance at various temperatures and for gases of various molecular weights is examined, it is found that a significant change in performance may occur. The turn-down ratio (maximum flow divided by minimum flow) of vortex valves decreases as temperature increases or as molecular weight decreases. Figure 5-7 shows the effect of a temperature increase on the performance of a one-inch vortex pressure amplifier as temperature is increased from room temperature to 1200°F.

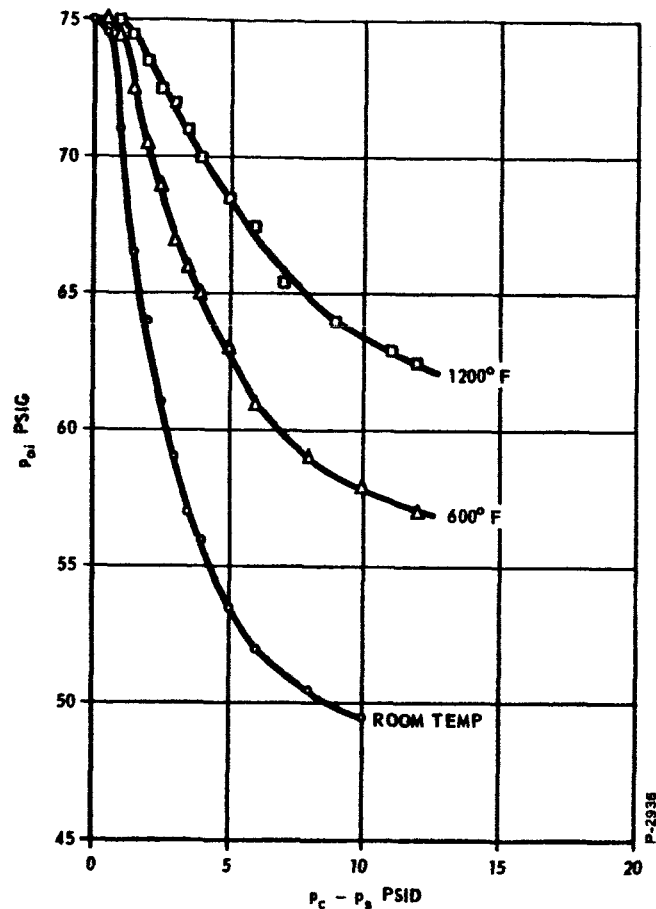


Figure 5-7 - Effect of Temperature of One Inch Vortex Pressure Amplifier at 75 Psig Supply Pressure

Equation (5-13) indicates that vortex amplifier performance at a given supply and exhaust pressure should be independent of gas density. It is therefore believed that the shift in performance is a Reynolds number effect. This is supported by the results of a recent test on the temperature sensitivity of a one-inch diameter pressure amplifier.

The results of this test were interpreted through use of the assumption that the expression for the Reynolds number of a vortex amplifier is given by:

$$N_R = \frac{12 \rho v_w D_1 g}{\mu} \quad (5-14)$$

where

N_R = Reynolds number - dimensionless

μ = dynamic viscosity - lb/sec-in

From equation (5-7) we can say that for the same pressure ratio:

$$v_c = K_c \sqrt{RT} \quad (5-15)$$

For the same pressure ratio, it is also reasonable to assume that

$$\frac{\dot{w}_c}{\dot{w}_o} = K_w \quad (5-16)$$

From equations (5-1), (5-5), (5-14), (5-15), and (5-16) we can then say that for a given vortex amplifier operating at a fixed pressure ratio

$$\frac{N_{R1}}{N_{R2}} = \frac{p_1 \mu_2}{p_2 \mu_1} \sqrt{\frac{(RT)_2}{(RT)_1}} \quad (5-17)$$

Figure 5-8 shows the maximum pressure gains obtained during the test of the 1-in. vortex pressure amplifier at various temperatures. The data has been plotted versus a relative Reynolds number taking the Reynolds number at 75 psig and room temperature as unity and using equation (5-17) to compute the remaining Reynolds numbers using p_s as the pressure.* Use of this equation is not strictly accurate since the value of $p_c - p_s$ at which the maximum gain occurs is not constant for a given value of p_s and varying temperatures. However, examination of equation (5-7) shows that the error is not great if $p_c - p_s$ is much smaller than p_s . The figure seems to show a definite relationship between Reynolds number and maximum pressure gain with a change in slope occurring at a relative Reynolds number of 0.43.

In the case of the neutron sensor, the working fluid is hydrogen which potentially may change in temperature from 200°R to 800°R. At 200°R and 1 atm, the viscosity of hydrogen is 2.54×10^{-7} lb/sec-in. while at 800°R it is 6.55×10^{-7} lb/sec-in.** From equation

* In these computations, viscosities were taken from Hilsenrath, Joseph, et. al. Tables of Thermal Properties of Gases, National Bureau of Standards Circular 564, November 1, 1955.

** Ibid

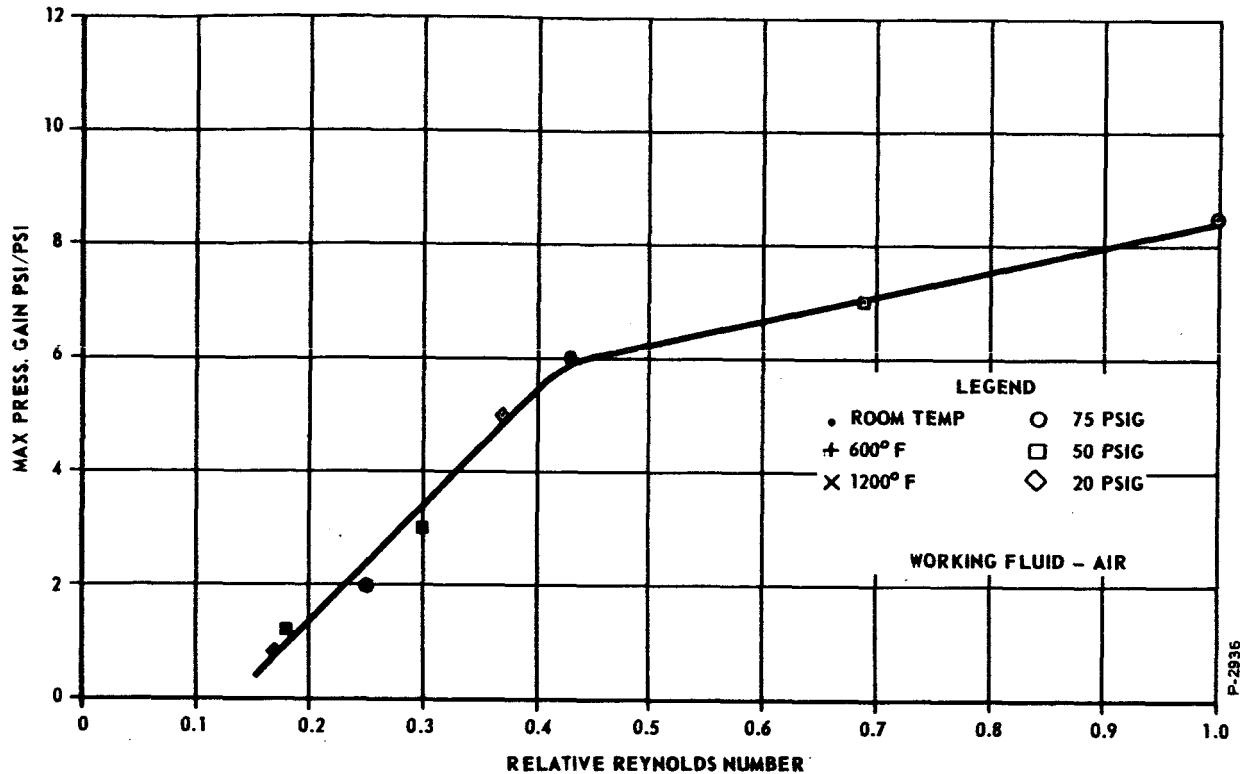


Figure 5-8 - Effect of Reynolds Number on Maximum Pressure Gain of a One Inch Diameter Vortex Amplifier

(5-17), the Reynolds number ratio corresponding to this range of temperatures and viscosities is 0.194.

Synthesis of a complete neutron sensor system will require use of low gain vortex amplifiers in the size range of 1-in. Use of equation (5-17) shows that the relative Reynolds number change from a vortex amplifier of this size operating on air at 520°R and $p_s = 89.7$ psia to hydrogen at 800°R and $p_s = 150$ psia is 0.542. Thus a 1-in. vortex amplifier operating at the neutron sensor environmental conditions giving the lowest Reynolds number would be in the region of lowest slope of Figure 5-8.

A 3-in. vortex amplifier operating at the same value of v_w as a 1-in. vortex amplifier would have a Reynolds number as defined by equation (5-14) three times greater. However, Figure 5-3 shows that the maximum gain of a 1-in. vortex amplifier with blocked output occurs at a value of $v_w \approx 30$ to 40 fps, while Figure 5-4 shows that the maximum gain of a 3-in. vortex amplifier occurs at $v_w \approx 9$ fps.

This indicates that angular velocity may be a significant parameter. The changes in v_w will cancel the effects of the diameter increase so that a 3-in. vortex amplifier at maximum gain will operate at a slightly lower Reynolds number as defined by equation (5-14) than a 1-in. amplifier at maximum gain, all other conditions being equal. However, it has not really been established that Reynolds numbers defined by equation (5-14) are equivalent for vortex amplifiers with different diameters. In addition, since a larger amplifier has a lower relative roughness and generally more accurate geometry, it is probably less sensitive to Reynolds number shifts than a smaller amplifier.

A complete evaluation of the temperature sensitivity problem would require experimental effort and is beyond the scope of the present investigation. Estimates of the relative Reynolds numbers indicate that the lowest Reynolds numbers of the neutron sensor vortex amplifiers will be above the range of greatest Reynolds number sensitivity. However, even though the sensitivity to Reynolds number may be expected to decrease as Reynolds number increases, test data indicates that the effect potentially could be great enough to significantly affect the accuracy of the neutron sensor. It should be kept in mind that the test data shown in Figure 5-7 and 5-8 comes from a device designed for room temperature operation and tested at elevated temperature. No attempt was made to alter geometry in order to optimize the device for operation at elevated temperature. It is believed that an effort to find a vortex amplifier geometry more favorable to high temperature operation would be successful. Furthermore, it is believed that compensation techniques can be devised which would overcome the effects of temperature shifts.

5.2.2 Supply Pressure Sensitivity

From equation (5-13), it can be seen that the pressure ratio, p_i/p_w , across an idealized vortex is a function of the supply to control pressure ratio, p_s/p_c , and the pressure ratio across the outlet orifice, p_e/p_u . If the outlet orifice is operated at pressure ratios less than the critical value (approximately 0.528 for a diatomic gas), the outlet pressure ratio is effectively the critical value, no matter what the actual values of the upstream and downstream pressures. Hence, when p_e/p_u is less than the critical value, the pressure ratio, p_i/p_w is essentially a function of p_s/p_c only, for a given vortex device. Also, for a given vortex device, there will be a consistent relationship

between the pressure ratio p_i/p_w and the output to supply pressure ratio p_o/p_s . We can therefore say that when p_e/p_u is less than the critical value, p_o/p_s will be a function of p_s/p_c . Then it can be shown that the pressure gain $K_p = \Delta p_o / \Delta (p_c - p_s)$ will be independent of p_s .

Figure 5-5 shows the pressure amplification characteristics of a high gain 3-in. diameter vortex amplifier. As can be seen from this figure, at p_s greater than 44.7 psia maximum gain is practically constant. (The difference between the gain of 3600 at $p_s = 44.7$ psia and the gain of 3000 at 54.7 psia can almost entirely be explained by the difficulty of accurately measuring the slope of a steep line.)

As can be seen from Figure 5-8, a 1-in. diameter low gain vortex pressure amplifier, tested at room temperature over the same range of p_s did exhibit a shift in maximum gain with change in p_s . This has already been attributed to a Reynolds number effect. Since, as has already been mentioned, a 3-in. and a 1-in. vortex amplifier will be operating at very nearly the same Reynolds number at the same value of p_s , it is indicated that the larger amplifier is less sensitive to Reynolds number shifts.

It may be concluded that the gains of the larger vortex amplifiers will be insensitive to shifts in supply pressure. The gains of the smaller vortex amplifiers may be sensitive to supply pressure variations because of the Reynolds number effect. However, it may be assumed that system supply pressure will be regulated in the neutron sensor application. Thus, the shifts in p_s will be a consequence of the inaccuracies and inconsistencies of the pressure regulators. These will be of a low magnitude and the shifts in Reynolds number, and hence pressure amplifier gain, will be slight.

Although the change in vortex amplifier gain with shifts in p_s will not be objectionable, the shift in the value of p_o with p_s may be more significant. Since a given percentage shift in p_s will cause approximately the same percentage shift in p_o , the vortex amplifier system will be no more accurate than its supply pressure regulation. Thus, precise supply pressure regulation is important if the overall system is to be accurate.

5.2.3 Effect of Control Port Area on Vortex Pressure Amplifier Gain

The overall gain of a vortex amplifier may be considered to be obtained by cascading three elemental gains. The first of these individual gains is that giving the change in p_o as a function of v_w . This gain, which has been discussed previously, is determined by the amplifier geometry and is affected by the physical size of the amplifier and by the Reynolds number. The second of these gains is that which results from the relationship between v_w and the control momentum $\dot{w}_c v_c / g$. This is a function of the control port diameter, D_c , and will be discussed in this subsection. The third of the cascaded gains is that associated with the pickoff and will be a function of the pickoff geometry.

From equation (5-6) we can say that for an idealized vortex:

$$\frac{p_w}{p_i} = f_3 \left(\frac{12 v_w}{\sqrt{gRT}} \right) \quad (5-18)$$

In a vortex amplifier, the pressure p_w will very closely approximate the vortex amplifier supply pressure, p_s . It can be assumed that for a given vortex amplifier, there will be a consistent relationship between p_i and the vortex amplifier output pressure, p_{oi} or p_{oe} . Then we can write:

$$\frac{p_{oi}}{p_s} = f_4 \left(\frac{12 v_w}{\sqrt{gRT}} \right) \quad (5-19)$$

Equation (5-19) may be differentiated for constant RT to obtain:

$$\Delta p_{oi} = 12 p_s K_v \frac{\Delta v_w}{\sqrt{gRT}} \quad (5-20)$$

where

$$K_v = \frac{d f_4 (v_w / \sqrt{gRT})}{d (v_w / \sqrt{gRT})}$$

Figure 5-6 shows that the control flow of a high gain pressure amplifier may be either greater than or less than the flow through the outlet orifice. Hence, we must consider two possibilities. We will first consider that in which $\dot{w}_o > \dot{w}_c$.

In this case, v_w is given by equation (5-1). Equation (5-1) assumes that the momentum exchange between the supply flow and the control flow is complete. There is considerable evidence to support the statement that the momentum exchange is not complete. However, since the final equation for gain will contain an experimentally determined value of K_v , which will take all inefficiencies of the vortex amplifier into account, no modification of equation (5-1) need be made at this point. In a high gain pressure amplifier, $p_c - p_s$ is much less than p_s so that v_c may be computed from equation (5-8) with little error and \dot{w}_c may be computed from:

$$\dot{w}_c = C_{dc} A_c \sqrt{\frac{2g p_s (p_c - p_s)}{RT}} \quad (5-21)$$

Substitution of equations (5-8) and (5-21) into equation (4-1) gives:

$$v_w = \frac{2C_{dc} A_c g (p_c - p_s)}{12 (\dot{w}_s + \dot{w}_c)} \quad (5-22)$$

A relationship defining the outlet flow, $\dot{w}_o = \dot{w}_c + \dot{w}_s$, must now be determined. Figure 5-9 shows the relationships between w_o and p_{oi} for vortex pressure amplifiers having various gains, and operated at sufficiently high supply pressures to insure that the pressure ratio across the outlet orifice is less than the critical pressure ratio. As can be seen, the outlet flow is always greater than the flow which would be computed using p_{oi} as the outlet orifice inlet pressure and an orifice coefficient determined at the maximum flow point. As gain increases, the sensitivity of \dot{w}_{oi} to p_{oi} decreases. From the figure, we can conclude that the relationship between \dot{w}_{oi} and p_{oi} will lie between two extremes. One of these extremes will be that of \dot{w}_o being completely insensitive to p_{oi} , i.e., \dot{w}_o is constant; the other will be that of p_{oi} being the effective inlet pressure for the outlet orifice.

In the case in which w_o is constant and $p_e/p_s < 0.528$,

$$\dot{w}_o = \dot{w}_s + \dot{w}_c = \frac{C_m A_2 C_{do} p_s}{\sqrt{RT}} \quad (5-23)$$

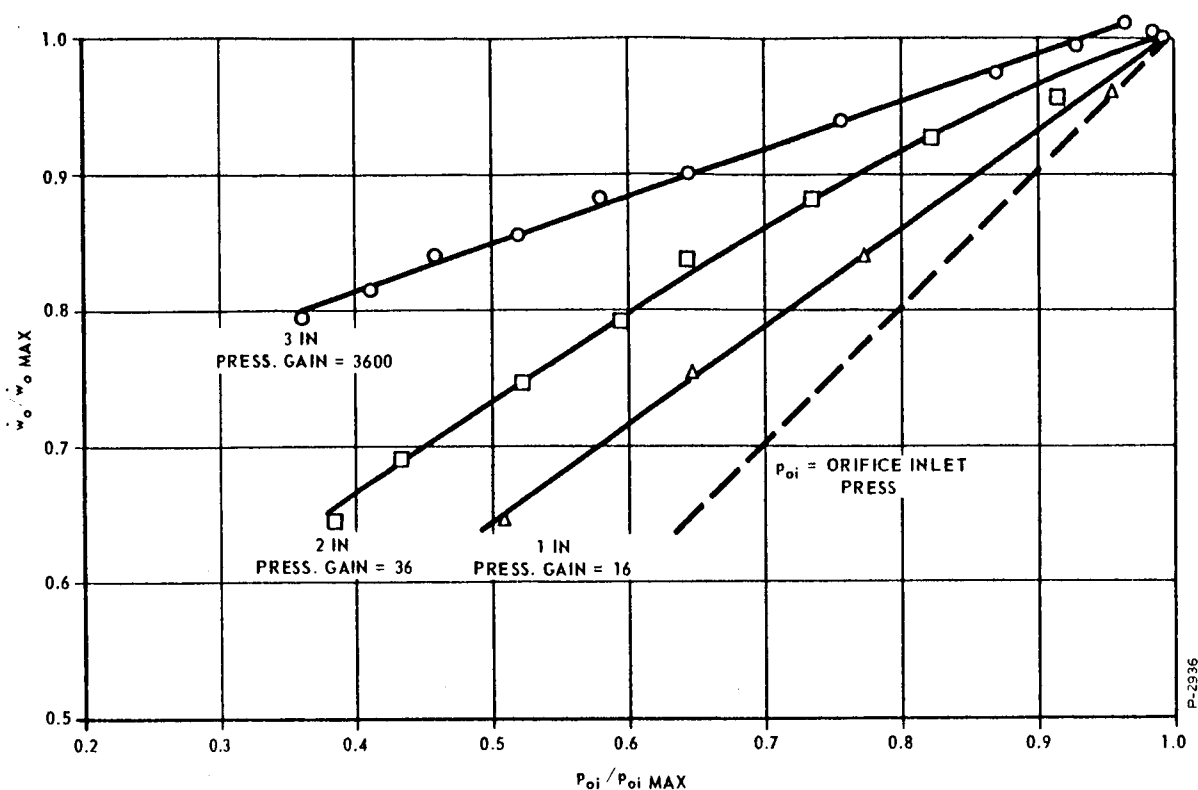


Figure 5-9 - Relation Between \dot{w}_o and p_{oi} for Vortex Amplifiers of Various Diameters at $p_s = 44.7$ Psia

where

$$C_m = \sqrt{g k \left(\frac{2}{k+1} \right)^{(k+1)/(k-1)}}$$

If p_{oi} defines the upstream pressure of the outlet orifice and if $p_e/p_{oi} < 0.528$, then:

$$\dot{w}_o = \frac{C_m A_2 C_{do} p_{oi}}{\sqrt{RT}} \quad (5-24)$$

Neither equation (5-23) or (5-24) exactly describes the true situation. Equation (5-23), which is based on the assumption of constant outlet flow, will be the most accurate in the case of a high gain pressure amplifier. Equation (5-24), which is based on the assumption that the flow through the outlet orifice is defined by an inlet pressure equal to p_{oi} , will be the most accurate in the case of a low gain pressure amplifier. The true case will be bracketed by these two equations.

Substitution of equation (5-23) into equation (5-22), and differentiating for constant p_s and RT gives:

$$\Delta v_w = \frac{2 C_{dc} A_c g \sqrt{RT} \Delta p_c}{12 C_m C_{do} A_2 p_s} \quad (5-25)$$

Substitution of equation (5-25) into equation (5-20) gives

$$\frac{\Delta p_{oi}}{\Delta p_c} = \left(\frac{2 \sqrt{g} K_v}{C_m} \right) \left(\frac{C_{dc} A_c}{C_{do} A_2} \right) \quad (5-26)$$

for the case in which \dot{w}_o is constant.

Substitution of equation (5-24) into equation (5-22), differentiating for constant p_s and RT , and linearizing about the quiescent point gives:

$$\Delta v_w = \frac{2 C_{dc} A_c g \sqrt{RT}}{12 C_m C_{do} A_2} \left[\frac{\Delta p_c}{p_{oi0}} - \frac{(p_{co} - p_s) \Delta p_{oi}}{p_{oi0}^2} \right] \quad (5-27)$$

Substitution of equation (5-27) into equation (5-20) gives:

$$\frac{\Delta p_{oi}}{\Delta p_c} = \frac{\frac{2 p_s K_v C_{dc} A_c \sqrt{g}}{C_m C_{do} A_2 p_{oi0}}}{1 + \frac{2 p_s K_v C_{dc} A_c \sqrt{g}}{C_m C_{do} A_2 p_{oi0}} \left(\frac{p_{co} - p_s}{p_{oi0}} \right)} \quad (5-28)$$

for the case in which p_{oi} is the outlet orifice upstream pressure and where p_{oi0} and p_{co} are the steady-state values of the pressures.

Equations (5-26) and (5-28) show that the value of $d p_{oi} / d p_c$ of a vortex amplifier will be very nearly proportional to the ratio $C_{dc} A_c / C_{do} A_2$. As the pressure gain of the amplifier increases, the proportionality between gain and the area ratio becomes more exact. Since A_2 cannot be changed without altering the geometry at the amplifier, and hence, K_v , the conclusion from equations (5-26) and (5-28) is that for $\dot{w}_c < \dot{w}_o$ and for a given K_v and A_2 , the value of $\Delta p_{oi} / \Delta p_c$ is approximately proportional to $C_{dc} A_c$. For constant p_s , $\Delta p_{oi} / \Delta p_c \approx K_p$.

The maximum possible pressure gain for a given chamber and pickoff geometry corresponds to the case in which $\dot{w}_o = \dot{w}_c$ at a point of maximum K_v . For this case we can say:

$$v_w = v_c$$

Substitution of equation (5-8) into the above equation gives:

$$v_w = \frac{1}{12} \sqrt{\frac{2 g R T}{p_s} (p_c - p_s)} \quad (5-29)$$

Equation (5-29) may be differentiated at constant RT and p_s to give:

$$d v_w = \frac{1}{12} \sqrt{\frac{2 g R T}{p_{so} (p_{co} - p_{so})}} \frac{dp_{co}}{2} \quad (5-30)$$

Substitution of equation (5-30) into equation (5-20) gives:

$$\frac{d p_{oi}}{d p_c} = \frac{K_v}{\sqrt{2}} \left(\frac{p_{co}}{p_{so}} - 1 \right)^{-1/2} \quad (5-31)$$

This gives the maximum value of $d p_{oi} / d p_c$ which can be obtained for any given values of K_v and p_c / p_s .

5.2.4 Effect of Pickoff

Two basic proportional pickoff configurations can be used in a vortex pressure amplifier. These are the internal and the external types whose general geometry is indicated in Figure 5-1.

The internal pickoff can be made to recover 100 percent of supply pressure at zero load flow and has a wide linear range of operation. Due to its construction and location, the noise level of the internal pickoff is low.

The best signal-to-noise ratio achieved to date by Bendix was obtained with a proportional external pickoff. It was found that the high pressure gain of the external pickoff improves the signal-to-noise ratio of the sensor beyond the value observed within the vortex chamber with internal pickoff. The improvement is due to changes in the sink flow region of the outlet; first, the continuous streamlines passing through the outlet orifice are straightened as the stream of flow passes through

the outlet hole which reduces the random fluctuations; and second, the increased gain due to the pickoff reduces the effect of unavoidable noise sources. The high signal gain of the external pickoff is obtained at the expense of pressure recovery and linear range. The external pickoff is also somewhat sensitive to geometrical inaccuracies and misalignments.

The use of an internal pickoff has been assumed in the present analysis. This assumption is conservative and has been made because of the greater amount of data available on both the pressure amplification and flow characteristics of vortex amplifiers with internal pickoffs.

The higher gains and more favorable noise characteristics of the external pickoff might lead to its use in the actual neutron sensor high gain amplifier. The reduced linearity and pressure recovery associated with this type pickoff might not be objectionable since pressure levels are high and a nonlinear output is desired in order to produce a logarithmic output from the sensor. However, any breadboard or prototype neutron sensor would have provision for the use of either pickoff and that configuration which gave the best overall performance would be used in the final design.

5.3 LOGARITHMIC OUTPUT AND RANGE CHARACTERISTICS

5.3.1 Estimate of Neutron Sensor High Gain Amplifier Gains and Flows

It will be assumed that the neutron sensor will use a high gain vortex amplifier having characteristics similar to those of the 3-in. vortex amplifier whose test data has been plotted in Figures 5-4, 5-5, and 5-6. Figure 5-4 shows that the maximum gain of this amplifier occurs with room temperature nitrogen at $v_w = 9$ fps. Taking vortex amplifier performance as being equivalent at equivalent values of $v_w / \sqrt{gRT} = M \sqrt{k}$ gives the value of v_w at maximum gain as $v_w = 21$ fps for 200°R hydrogen and $v_w = 42$ fps for 800°R hydrogen. The value of K_v may be estimated from Figure 5-4 as 59.

It can be assumed that the high gain vortex amplifier used in the neutron sensor will be constructed with an A_c/A_2 ratio which will lie between two extremes. One of these will be equivalent to the 3-in. vortex amplifier whose test data is presented in this report. The other will be the A_c/A_2 ratio which gives the highest pressure gain. This corresponds to the case in which all incoming flow passes through the control ports at the maximum value of K_v .

If all incoming flow is supplied through the control ports, the value of $p_c - p_s$ required to obtain the value of v_w corresponding to the maximum gain may be computed from equation (5-29). For $v_w = 21$ fps in 200°R hydrogen, the calculated pressure drop is 0.0067 psi. The same pressure drop will give a value of $v_w = 42$ fps at 800°R.

The maximum gain of a vortex amplifier operating with all flow supplied through the control ports may be estimated from equation (5-31). For small values of $p_c - p_s$, a more convenient form of this equation is:

$$\frac{\Delta p_{oi}}{\Delta p_c} = K_v \sqrt{\frac{p_s}{2(p_c - p_s)}} \quad (5-32)$$

For $K_v = 59$, $p_s = 150$ psia, and $p_c - p_s = 0.0067$ psi, equation (5-32) gives $\Delta p_{oi}/\Delta p_c = K_p = 6200$ for a constant p_s .

As previously stated, the maximum gain of a vortex amplifier operating with less than critical pressure ratio across the outlet orifice will tend to be independent of the supply pressure. A vortex amplifier

proportioned as the 3-in. amplifier whose test data has been given in this report will then have a pressure gain of approximately 3000.

Thus, we can estimate that the high gain amplifier used in the neutron sensor will have pressure gains in the range of 3000 to 6200. These estimates are conservative, since the value of K_v will, if not a constant, increase with pressure, and since an external pickoff would give a higher gain.

The flows for a vortex amplifier operating at a gain of 3000 on hydrogen may be estimated from Figure 5-6. At the point of maximum gain, $\dot{w}_c/\dot{w}_o = 0.55$. Thus, from equation (5-1), $v_w = 0.55 v_c$ at the maximum gain point. Equation (5-8) gives $p_c - p_s = 0.022$ psi for $v_w = 21/0.55 = 38$ fps, $p_s = 150$ psia and $T = 200^\circ\text{R}$. For $A_c C_{dc} = 0.088$ in², which is the measured value for the actual amplifier, this pressure drop gives $\dot{w}_c = 0.033$ lb/sec of hydrogen at 200°R and 0.016 lb/sec of hydrogen at 800°R . The corresponding values of \dot{w}_o are 0.006 lb/sec and 0.0029 lbs/sec of hydrogen.

Noise levels on the order of 1-in. of $\text{H}_2\text{O} = 0.036$ psi measured at the output have been achieved in high gain vortex sensor applications. Dividing 0.036 psi by 3000 to 6200 indicates a minimum detectable change of control pressure in the range of 6×10^{-6} psi. It will be assumed that the minimum detectable value of ion pump output pressure, p_p , is 10^{-5} psid. Then if the low range amplifier of the neutron sensor operates over three decades of input range, p_p will vary between 10^{-5} and 10^{-2} psid; for four decades of input, p_p will range between 10^{-5} and 10^{-1} psid. For the case in which all incoming vortex amplifier flow passes through the control ports, for a three decade range of input, \dot{w}_c will increase by a factor of $\sqrt{(0.0066 + 0.01)/(0.0066)} = 1.59$. For the case in which \dot{w}_c is approximately 55 percent of \dot{w}_o at the maximum gain point, \dot{w}_c will increase by a factor of $\sqrt{(0.022 + 0.1)/(0.022)} = 2.35$ for four decades of input. From Figure 5-6, the value of \dot{w}_o may be expected to decrease 20 to 30 percent over the range of the amplifier.

Table 5-2 summarizes the results of the estimates of the flow demands for a high gain vortex amplifier in the neutron detector application. The data in the table brackets the weight flows for the contemplated extremes of gain and temperature. Negative values of \dot{w}_s indicate a reverse (away from amplifier) supply flow.

Table 5-2 - Estimates of Flow Demands for High Gain Amplifier with $C_{dc} A_c = 0.088 \text{ in}^2$

v_w/v_c	T °R	p_p psi	$(p_c - p_g)$ psi	\dot{w}_c lb/sec	\dot{w}_o lb/sec	\dot{w}_g lb/sec
1	200	10^{-5}	0.0066	0.006	0.006	0
	200	10^{-2}	0.0166	0.0095	0.0045	-0.005
0.55	200	10^{-5}	0.022	0.0033	0.0060	0.0027
	200	10^{-1}	0.122	0.0078	0.0045	0.0035
1	800	10^{-5}	0.0066	0.0029	0.0029	0
	800	10^{-2}	0.0166	0.0046	0.0022	-0.0024
0.55	800	10^{-5}	0.022	0.0016	0.0029	0.0013
	800	10^{-1}	0.122	0.0038	0.0022	-0.0022

P-2936

5.3.2 Theoretical Gains Required to Obtain a Logarithmic Output

If the output of the neutron sensor system is to be a mathematically exact logarithm of the neutron flux, the following relationship will hold for values of ϕ between the minimum and maximum values:

$$p_{oi} = p_{oi_{min}} - \frac{(p_{oi_{max}} - p_{oi_{min}})}{N} \log \left(\frac{\phi}{\phi_{max}} \right) \quad (5-33)$$

where

N = number of decades of neutron flux to be detected = $\log(\phi_{max}/\phi_{min})$ - dimensionless

ϕ = neutron flux - neutrons/cm² sec

Differentiation of equation (5-33) gives:

$$\frac{dp_{oi}}{d\phi} = \frac{-(p_{oi_{max}} - p_{oi_{min}})}{N \phi} \log(e) \quad (5-34)$$

where

$$\log(e) = 0.43429$$

Until suitable experimentation is performed, the exact form of the relationship between the ion pump output pressure, p_p , and the neutron flux, ϕ , will not be known. The logarithmic characteristic must be obtained through a matching of the nonlinearities of the ion pump and the vortex amplifier circuitry. When the nonlinearities of the ion pump are accurately defined, an accurate prediction of the ability of the complete neutron sensor system to produce a logarithmic output can be performed. In order to perform a preliminary investigation of the ability of a vortex amplifier to produce a logarithmic output, it will be assumed that the output ion pump is a linear function of the neutron flux:

$$p_p = K_i \phi \quad (5-35)$$

Substitution of equation (5-35) into equation (5-34) gives:

$$\frac{d p_{oi}}{d p_p} = \frac{-0.43429 \left(p_{oi_{\max}} - p_{oi_{\min}} \right)}{N p_p} \approx K_p \quad (5-36)$$

Equation (5-36) may be used to compute the gain required to obtain a given range of logarithmic output pressure for a given number of decades of input pressure starting at a specific input pressure. This equation may also be used to compute the range of output pressure for a logarithmic output for a given number of decades of input starting with a specified pressure gain and input pressure.

5.3.3 Logarithmic Characteristics of High Gain Vortex Amplifiers

Equation (5-36) may be used to estimate the range of output pressures which can be obtained from a logarithmic amplifier having the maximum gain characteristics estimated for a 3-in. diameter vortex amplifier in subsection 5.3.1. For $K_p = 6200$, $N = 3$, and $p_p = 10^{-5}$ psi, $(p_{oi_{\max}} - p_{oi_{\min}}) = 0.43$ psi from equation (5-36). For $K_p = 3000$, $N = 4$, and $p_p = 10^{-5}$ psi, $(p_{oi_{\max}} - p_{oi_{\min}}) = 0.28$ psi.

The above results show that extremely high gains are required if a logarithmic amplifier is to produce a wide range of output pressure for small input signal levels. High gain amplifier output signal ranges of less than one psi may be satisfactory if the neutron sensor is to be used purely as instrumentation. However, if the neutron sensor is to be used to drive some other pneumatic component, a larger

output pressure range would be highly desirable. Some deviation from the ideal logarithmic characteristics will have to be accepted at the low input levels if an output pressure range above one psi is required.

Figure 5-10 shows the output of the 3-in. vortex amplifier at $p_s = 44.7$ psia for an assumed bias pressure of 0.0075 psia plotted on a logarithmic scale. As can be seen, for limited ranges, the output pressure approximates a logarithmic function of the input pressure. However, the gain at the low ranges of input is too low and the gain at the high ranges of input is too high compared with that of a theoretical logarithmic function covering the whole range.

There is little that can be done presently about increasing the gain at the low levels of input. Estimates made in subsection 5.3.1 predict gains in the range of 3000 to 6200 for a 3-in. vortex pressure amplifier. This is in the range of experimentally demonstrated pressure gains. Some improvement in gain can be obtained with the external pickoff and by increasing the amplifier diameter. However, the increase in gain required here is a factor of 10 or better, and this appears to be beyond the capabilities of the present state of vortex amplifier technology without going to unreasonably large vortex amplifier diameters.

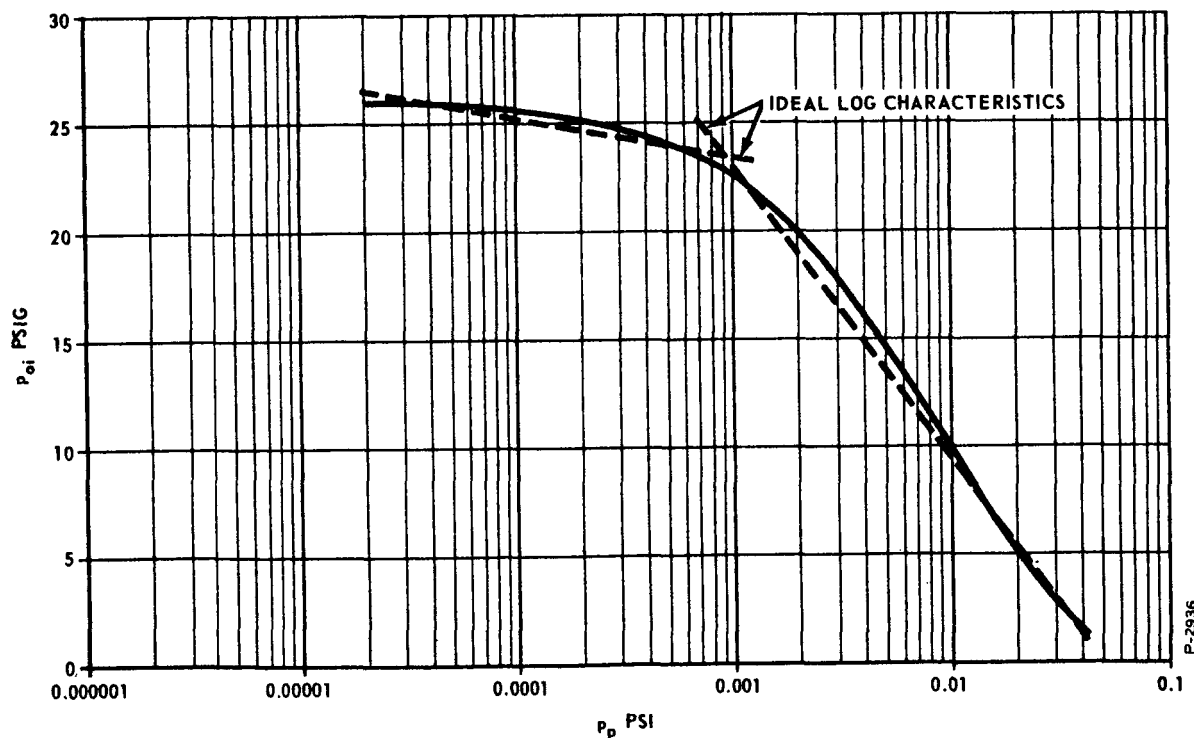


Figure 5-10 - Logarithmic Characteristics of a Three Inch Vortex Amplifier with a 0.0075 Psi Bias Pressure

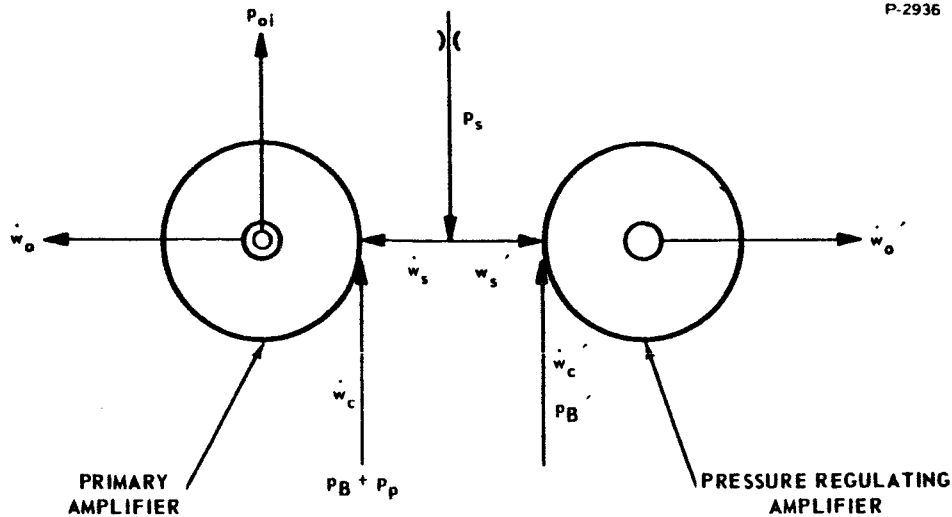


Figure 5-11 - Approach to Logarithmic Vortex Amplifier

On the other hand, decreasing the gain at the higher levels of signal input presents no fundamental difficulty. Figure 5-11 depicts one approach that can be used to achieve this goal. Here a pressure regulating amplifier is used to maintain the supply pressure, p_s , of the primary amplifier. With no signal pressure, p_p , the pressure regulator is set at an operating point corresponding to a very small pressure regulator supply flow, \dot{w}_s' . As p_p is increased, \dot{w}_c increases and the primary output amplifier supply flow \dot{w}_s decreases. As \dot{w}_s decreases \dot{w}_s' must increase. However, the action of the pressure regulating amplifier is such that very small increases in p_s generate relatively large increases in \dot{w}_s' . As p_s approaches the level of p_B' , larger increases in p_s are required to generate a given increase in \dot{w}_s' . Once $p_s \geq p_B'$, the pressure regulating amplifier will act as a fixed orifice.

By proper selection of the values of p_B' , \dot{w}_c' , and \dot{w}_s' corresponding to $p_p = 0$, it will be possible to maintain p_s at a very nearly constant value for the lowest ranges of p_p where a high primary amplifier gain is needed. As p_p increases into its higher ranges, the ability of the pressure regulating amplifier to maintain p_s at a nearly constant value will decrease. As p_s increases, p_{Oi} will increase in proportion and the apparent effect will be a decrease in the gain of the primary amplifier. The end result will be to make the saturation curve of the primary amplifier more nearly approximate the logarithm of the input.

The circuit represented in Figure 5-11 is fairly complex. Performance depends upon the relative magnitudes of a number of variables. Evaluation of the degree of accuracy with which a logarithmic output can be approximated would best be achieved by testing of a bread-board circuit. This effort is beyond the scope of the present project.

However, some idea of the accuracy with which a logarithmic function can be approximated by the saturation curve of a vortex pressure amplifier can be derived from Figure 5-10. Consider the range of input pressures between 0.001 and 0.04 psi. The maximum deviation from the ideal logarithmic characteristic occurs at an input pressure of approximately 0.0035 psi. The maximum deviation is 1.2 psi. Since the output pressure range corresponding to the input range of 0.001 to 0.04 psi is 24 psi, the maximum output deviation is 5 percent. This is probably a fair estimate of the accuracy with which the saturation curve of a vortex amplifier approximates a logarithmic function. The data of Figure 5-10 was not taken for the purpose of obtaining a logarithmic output and no attempt was made to modify the amplifier to improve its logarithmic characteristics.

A greater deviation from the desired characteristics will occur at the lowest input levels where vortex amplifier gains will not be high enough to maintain the logarithmic characteristic. An estimate of the magnitude of this deviation can be made by assuming that the vortex amplifier is linear over the lowest decade of input.

From equation (5-36) the theoretical gain of a logarithmic amplifier in psi/decade is

$$K_L = \frac{p_{oi_{max}} - p_{oi_{min}}}{N} = \frac{p_p K_p}{0.434} \quad (5-37)$$

where K_p is the pressure gain corresponding to a given value of p_p .

If the device is to be linear over the lowest decade and logarithmic over all other decades, K_L may be computed from:

$$K_L = \frac{10 p_{p_{min}} K_{p_{max}}}{0.434} \quad (5-38)$$

since $K_p = K_{p_{max}}$ over the lowest decade of p_p .

If the amplifier is linear over its lowest decade of input, the output pressure change over this input range will be

$$\Delta p_L = K_{p_{\max}} (10 p_{p_{\min}} - p_{p_{\min}}) = 9 K_{p_{\max}} p_{p_{\min}} \quad (5-39)$$

The pressure error at the lowest value of p_p will then be:

$$\text{Error} = K_L - \Delta p_L \quad (5-40)$$

and the error expressed as a percent of the total theoretical range will be

$$\text{Percent Error} = \frac{\text{Error}}{NK_L} \times 100 \quad (5-41)$$

Substitution of equations (5-38) through (5-40) into equation (5-41) gives:

$$\text{Percent Error} = \frac{61}{N} \quad (5-42)$$

Equation (5-42) is a perfectly general expression which gives the maximum deviation (expressed as a percentage of the theoretical range) from the theoretical logarithmic characteristic for an amplifying device which is linear over the lowest decade of input, and logarithmic over all others.

The operation of the amplifier on a linear part of its operating curve at the low input signal levels has an advantage in addition to the increase in the output range. Noise in a nonlinear amplifier will cause an apparent null shift because of the fact that noise pulses on one side of the signal are amplified more than those on the other. Since noise level is variable, the effect is that of a variable null. This effect is aggravated as the signal-to-noise ratio decreases and as the amplifier becomes more nonlinear. Hence, operating the amplifier on a linear portion of its curve at the lowest signal levels will minimize this effect.

Figure 5-12 is a sketch summarizing the estimates of the accuracy with which a vortex amplifier can approximate a logarithmic function for the neutron sensor application (a closer approximation is possible in an application involving high level input signals). This shows the probable error of 5 percent over the region where the vortex amplifier is operated on its saturation curve with the maximum error occurring at the minimum input which is a consequence of operating the amplifier on the linear part of its operating curve.

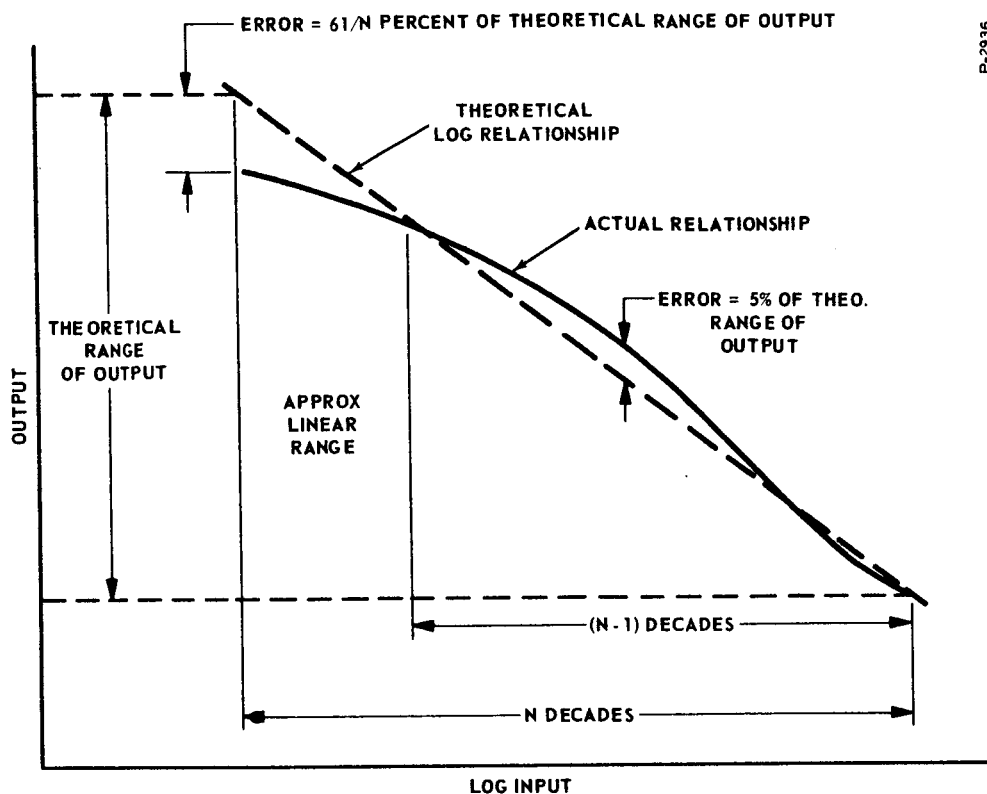


Figure 5-12 - Approximation of Logarithmic Function

5.4 DYNAMIC RESPONSE CHARACTERISTICS

5.4.1 Estimate of High Gain Vortex Amplifier Dynamics

The dynamic performance of any pneumatic device depends upon the length of time required for energy storage elements to change their energy level and upon transport delays involving propagation of pressure and flow. In the case of the vortex amplifier, the energy storage aspect involves the change in accumulated mass within the chamber as the pressure profile of the vortex changes. Transport delay is encountered in that a step change in control output couples in a tangential velocity at a stream tube adjacent to the input and time is required for this effect to propagate through the vortex chamber; in other words, a discrete time is required for the velocity profile to reach a new equilibrium.

It is conservative to say that the transport delay is simply the filling time of the vortex chamber or that time required to completely exchange the fluid in the chamber with new fluid. This is:

$$h = \frac{V_{p_v}}{\dot{w}_{oo} RT} \quad (5-43)$$

where

h = transport delay - sec $\pi D_1^2 l$

V = vortex chamber volume $\frac{1}{4}$ - in³

\dot{w}_{oo} = quiescent flow from vortex chamber outlet - lb/sec

p_v = average pressure in vortex chamber - psia

Precise evaluation of the average chamber pressure, p_v , requires integration of the pressure profile across the vortex chamber. This pressure profile is not accurately known. Quite obviously it will be conservative to assume that $p_v = p_s$. Thus we can say:

$$h_{\max} = \frac{V p_s}{\dot{w}_{oo} R T} \quad (5-44)$$

In the usual vortex amplifier, l is equal to or greater than the diameter of the outlet hole, D_2 . This insures that the major restriction to \dot{w}_o is the outlet orifice area $\pi D_2^2/4$ rather than the cylindrical area $\pi D_2 l$. Thus, the chamber volume, V , may be reduced as the value of \dot{w}_o , and hence the required value of D_2 , decreases.

From Table 5-2, the minimum value of \dot{w}_o for $T = 200^\circ R$ (corresponding to $K_p \approx 3000$) is 0.0045 lb/sec. The outlet orifice diameter corresponding to this value of \dot{w}_o is roughly 0.09 in. The chamber volume, V , for $l = D_2$ is then 0.64 in³. Substituting these values with $p_s = 150$ psia and $R = 9250$ in/[°]R into equation (5-44) gives $h_{\max} = 0.012$ sec.

The energy storage aspect of the vortex chamber is simply the time required for sufficient mass to flow from or into the chamber to permit establishment of a new pressure profile across the chamber. It can be assumed that changes in the control input generate a weight flow immediately after the transport delay. This, again, is a conservative assumption. The accumulation or loss of mass in the vortex chamber can then be described by:

$$\frac{V}{k R T} \frac{dp_v}{dt} = \dot{w}_w - \dot{w}_o \quad (5-45)$$

where

\dot{w}_w = flow entering vortex chamber at outer radius - lb/sec

t = time-sec

A relationship is now needed between p_v and \dot{w}_o . A clue to this relationship is offered by Figure 5-9 which shows an almost perfectly linear relationship between p_{oi} and \dot{w}_o of the form:

$$\dot{w}_o = W_o + k_o p_{oi} \quad (5-46)$$

where

W_o = outlet flow intercept - lb/sec

k_o = outlet flow slope - in²/sec

Differentiating equations (5-45) and (5-46), linearizing, and taking Laplace transforms gives:

$$\frac{Vs \Delta p_v}{k R T} = \Delta \dot{w}_w - \Delta \dot{w}_o \quad (5-47)$$

$$\Delta \dot{w}_o = k_o \Delta p_{oi} \quad (5-48)$$

Making the conservative assumption that $p_v = p_o$ and combining equations (5-4) and (5-48) gives:

$$\frac{\Delta p_o}{\Delta \dot{w}_w} = \frac{1/k_o}{\frac{Vs}{k_o k R T} + 1} \quad (5-49)$$

This is of the form:

$$\frac{\Delta p_o}{\Delta \dot{w}_w} = \frac{K}{\tau s + 1} \quad (5-50)$$

where τ = the vortex chamber time constant given by:

$$\tau = \frac{V}{k_o k R T} \quad (5-51)$$

From Figure 5-9, it can be ascertained that k_o for the 3-in. high gain amplifier is:

$$k_o = \frac{0.3 \dot{w}_{\max}}{p_{oi\max}} \quad (5-52)$$

Substituting equation (5-52) into equation (5-51) gives:

$$\tau = \frac{V p_{oi\max}}{0.3 \dot{w}_{o\max} k R T} \quad (5-53)$$

From Table 5-2, $\dot{w}_{o\max} = 0.006 \text{ lb/sec}$ for $T = 200^\circ\text{R}$. Substituting this value with $k = 1.4$, $p_{oi\max} = 150 \text{ psia}$, and $R = 9250 \text{ lb}_m\text{-in}/^\circ\text{R lb}_f$ into equation (5-53) gives $\tau = 0.021 \text{ sec}$.

Experimental measurements of the dynamic response of a vortex amplifier indicate that the estimate of the value of τ given by equation (5-53) will be quite accurate. The same measurement indicates that the value of h given by equation (5-44) will be considerably larger than the true value. In one specific case, calculated values of h were three times larger than measured values.

It is desired that the neutron sensor have a time constant of 0.02 sec which gives a total time of 0.06 sec to reach 95 percent of the output change corresponding to a given input step change. If both a single order lag and a transport delay are present, the time to reach 95 percent of the final output change in response to a step change in input is given by:

$$t_R = h + 3\tau \quad (5-54)$$

where

$$t_R = \text{response time - sec}$$

The values of h_{\max} and τ just estimated give $t_R = 0.012 + 3(0.021) = 0.075 \text{ sec}$, which is greater than the desired 0.060 sec.

There are a number of ways in which one might attempt to improve the dynamic response of a vortex amplifier. Basically, we can decrease V and p_{oi} or we can increase \dot{w}_o . A decrease in V by decreasing D_1 alone implies a decrease in gain since the ratios D_2/D_1 and

D_{oi}/D_1 are decreased. A decrease in D_1 accompanied by a corresponding reduction in D_2 gives no advantage, since V and \dot{w}_o change proportionately. Too great a decrease in ℓ will have a destructive effect on amplification. Attempting to increase response by reducing p_{oi} implies a reduction in the general pressure level of the neutron sensor system. Such a reduction cannot be made without reducing \dot{w}_o unless the diameter D_2 is increased. Again, this has an adverse effect on gain. Thus, as might be expected, high gain and fast response are somewhat conflicting requirements. One approach that can be taken to the problem of obtaining fast response while maintaining high gain is to operate the vortex amplifier at as high a ratio \dot{w}_c/\dot{w}_o as is possible while increasing the area A_2 to get the desired response. The losses in chamber gain can be at least partially made up by the increase in control port gain.

It has already been indicated that the estimate of transport delay based on equation (5-44) is undoubtedly significantly pessimistic. In one specific case, the estimate from the equation was three times too large. If we take $h_{max} = 0.004$ sec, which is one third of the value estimated from equation (5-44) for $T = 200^\circ R$, and retain the estimated value of $\tau = 0.021$ sec, equation (5-54) gives $t_R = 0.067$ sec. Only slight improvements in estimated response are required to obtain values less than 0.06 sec. Thus, we conclude that the desired dynamic response can be obtained in a single high gain vortex amplifier with a pressure gain of approximately 3000.

It should be noted that any problems with dynamic response will be most critical at the lowest temperatures. Since \dot{w}_o is inversely proportional to \sqrt{T} while t_R is inversely proportional to T for a given \dot{w}_o , the net effect is that t_R is inversely proportional to \sqrt{T} . Thus, the increase in temperature from $200^\circ R$ to $800^\circ R$ will cut dynamic response time in half.

5.4.2 Estimate of Dynamics Downstream of High Gain Vortex Amplifier

If the ion pump output pressure is a perfectly linear function of the neutron flux, at least two primary vortex amplifiers will be needed to cover the detectable neutron flux range. The outputs of these primary amplifiers must be added to obtain a single output which will be a function of the neutron flux. The addition can be performed with a 1-in. diameter vortex amplifier which will have dynamic response characteristics which must be considered as part of the dynamic response of

the overall neutron sensor system. Furthermore, an interconnecting channel between the output of the high gain amplifier and the input of the adding amplifier may have significant dynamics. A schematic of two cascaded vortex amplifiers and a block diagram indicating the notation for the dynamics is shown in Figure 5-13.

If the internal pickoff is used, the pickoff diameter, D_{oi} , will be quite small. The adding amplifier will be immediately adjacent to the primary amplifier. Thus, the length of the connecting channel will be quite small. In view of these facts, little error is introduced by treating the dynamics of the connecting channel on the basis of a lumped resistance-capacitance circuit.

We can write the following equation for the connecting channel:

$$\dot{w}_{oi} = \dot{w}_{c3} + \frac{d w_2}{d t} \quad (5-55)$$

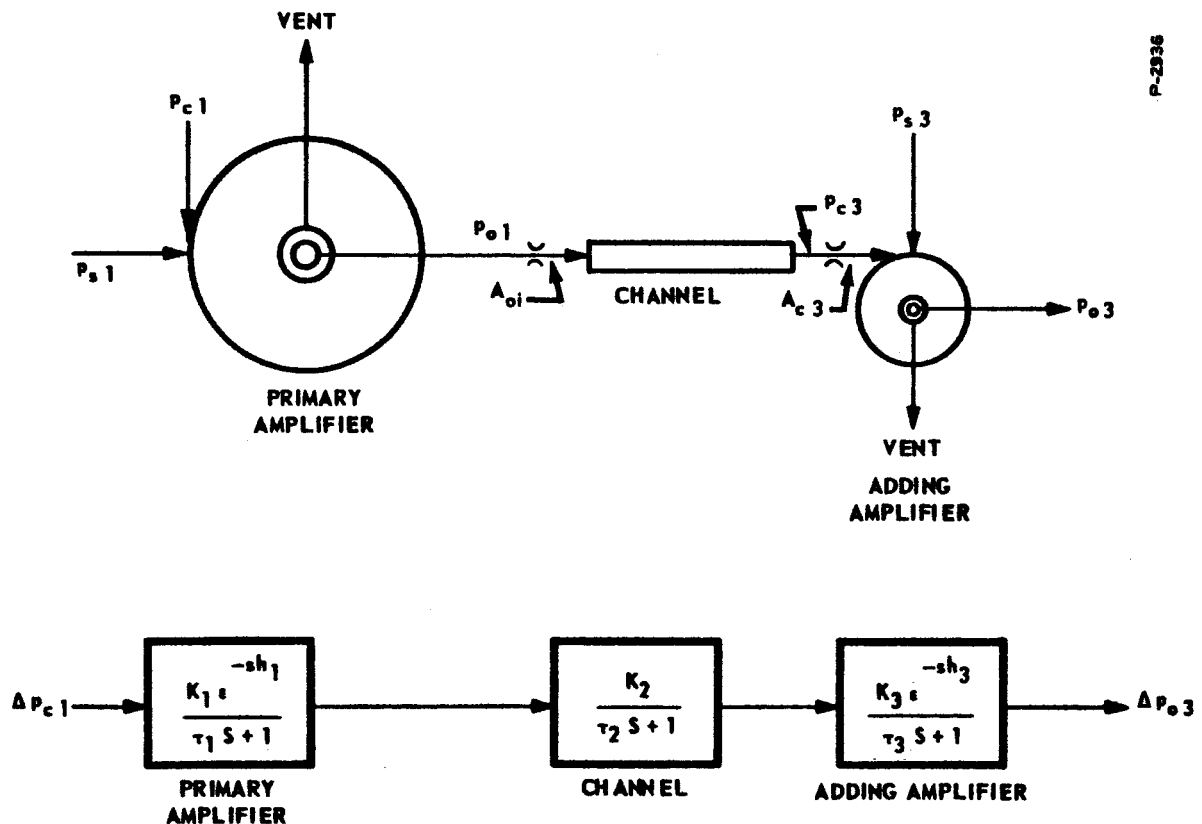


Figure 5-13 - Cascaded Vortex Amplifiers

where

\dot{w}_{o1} = flow through output pressure tap of primary amplifier - lb/sec

\dot{w}_{c3} = control flow into adding amplifier lb/sec

$\frac{dw_2}{dt}$ = accumulation of gas within channel - lb/sec

If we assume that the pressure in the channel is less than $0.528 p_o$, we can write

$$\dot{w}_{o1} = \frac{C_{d o1} A_{o1}}{\sqrt{R T}} p_{o1} \sqrt{g^k} \left(\frac{2}{k+1} \right)^{(k+1)/2(k-1)} \quad (5-56)$$

Also:

$$\frac{dw_2}{dt} = \frac{V dp_{c3}}{k R T dt} \quad (5-57)$$

The flow \dot{w}_{c3} will be given by an appropriate form of the compressible flow equation or a suitable approximation. Using either the incompressible flow or the Fliegner equation, we obtain

$$\Delta \dot{w}_{c3} = \frac{\dot{w}_{c30}}{2(p_{c30} - p_{s3})} \Delta p_{c3} \quad (5-58)$$

In equation (5-58), the zero subscripts indicate the quiescent values of the variables.

Differentiation of equations (5-56) and (5-57), linearizing, and taking Laplace transforms gives:

$$\Delta \dot{w}_{o1} = \frac{\dot{w}_{o10}}{p_{o10}} \Delta p_{o1} \quad (5-59)$$

$$s \Delta w_2 = \frac{V_c s \Delta p_{c3}}{k R T} \quad (5-60)$$

Substitution of equations (5-58), (5-59), and (5-60) into equation (5-55) gives:

$$\frac{\dot{w}_{o10}}{p_{o10}} \Delta p_{o1} = \frac{\dot{w}_{c30} \Delta p_{c3}}{2(p_{c30} - p_{s3})} + \frac{V_c s \Delta p_{c3}}{k R T} \quad (5-61)$$

since $\dot{w}_{o10} = \dot{w}_{c30}$

$$\Delta p_{c3} = \frac{2(p_{c30} - p_{s3})/p_{o10}}{\frac{2V_c (p_{c30} - p_{s3})}{k R T \dot{w}_{o10}} s + 1} \quad (5-62)$$

or:

$$K_2 = 2(p_{c30} - p_{s3})/p_{o10} \quad (5-63)$$

and

$$\tau_2 = \frac{2V_c (p_{c30} - p_{s3})}{\dot{w}_{o10} k R T} \quad (5-64)$$

from which:

$$\tau_2 = \frac{K_2 V_c p_{o10}}{k R T \dot{w}_{o10}} \quad (5-65)$$

Substitution of equation (5-56) into equation (5-65) gives:

$$\tau_2 = \frac{K_2 V_c}{k C_{do} A_{031} \sqrt{g k R T}} \left(\frac{k+1}{2} \right)^{(k+1)/2(k-1)} \quad (5-66)$$

For $D_{03} = 0.02$ in., $A_{031} = 3.1 \times 10^{-4}$ in². We can assume that the inter-connecting channel will be no longer than 2-in. and will have a diameter no greater than 0.1 in. For these dimensions, $V_c = 0.016$ in³. Substitution of these values, with $k = 1.4$, $C_{d3} = 0.6$, $g = 386$ in/sec², $R = 9250$ in-lb_m/lb_f°R, and $T = 200^\circ R$ into equation (5-66) gives

$$\tau_2 = 0.0032 K_2 \quad (5-67)$$

As can be seen by equation (5-63), K_2 must, by its very nature, be less than 1. The exact value of K_2 will depend upon the relative impedances of the primary amplifier and the adding amplifier. The type of impedance match will depend upon the type of load which the neutron sensor is to drive. Proper matching of the impedances of the two amplifiers is a detailed task which is beyond the scope of the present feasibility study. However, we can make an order of magnitude estimate of K_2 .

A fairly low gain 1-in. vortex pressure amplifier will have a maximum gain at a value of $p_{c3} - p_{s3}$ no greater than 5 psid at values of $p_{s3} \approx 50$ psia. For this value of $p_{c3} - p_{s3}$ and $p_{o1} = 150$ psia, equation (5-63) gives $K_2 = 0.067$ which from equation (5-67) gives $\tau_2 = 0.0002$ sec. As the gain of the adding amplifier increases, the value of $p_{c3} - p_{s3}$ must come down. Thus, we can conclude that if the adding amplifier is a pressure amplifier, τ_2 will be small enough to be neglected providing that the channel dimensions are no greater than those assumed here.

If the neutron sensor drives a load which requires a flow input, rather than a pressure input, the adding amplifier will be a flow amplifier rather than a pressure amplifier. Under these circumstances, the value of $p_{c3} - p_{s3}$ will be greater than 5 psid. However, systems with $K_2 > 0.5$ do not appear to be likely, so that τ_2 will never be greater than 0.0016 sec.

The dynamics of the 1-in. adding amplifier will be described by equations in the form of (5-44) and (5-53). The outlet orifice may be expected to have a diameter of 0.020 to 0.050 in, where the smaller dimension would be typical of a higher gain pressure amplifier and the larger dimension would be typical of a lower gain pressure amplifier. The dimension, l , will not be less than 0.05 in. as a practical matter. Thus V will be 0.039 in^3 . We may assume that the supply pressure of the adding amplifier will be 50 psia. From Figure 5-9, we can estimate that

$$k_o = 0.7 \frac{\dot{w}_{o_{\max}}}{p_{o_{\max}}} \quad (5-68)$$

for a 1-in. vortex amplifier. We can estimate that $\dot{w}_{o_{\max}} = 10^{-4} \text{ lb/sec}$ if $D_2 = 0.02$ in. and that $\dot{w}_{o_{\max}} = 6.25 \times 10^{-4} \text{ lbs/sec}$ if $D_2 = 0.05$ in. Using these values and the values of the other parameters corresponding to $T = 200^\circ\text{R}$ gives a range of τ_3 of 0.0017 to 0.011 sec. The values of

h_{\max} will be somewhat less. The higher value of τ_3 corresponds to a 1-in. diameter pressure amplifier with fairly high gain; the lower value of τ_3 corresponds to a low gain amplifier.

We can conclude that any attempt to boost the overall system gain with the adding amplifier will have a significant effect on the response of the system and should probably be avoided. The matching of the two vortex amplifiers to obtain the optimum gain and response requires more definition of the load that the neutron sensor will drive than is presently available.

The effect of vortex amplifier dynamics on neutron sensor response will be discussed further in Section 6.3.

5.5 NOISE CHARACTERISTICS

Noise is a factor which cannot be ignored in any application which involves the use of high gain pneumatic amplifiers working on low level signals. Noise is a highly complex phenomenon and an independent noise study requires an extensive undertaking which to a large extent must be based on experiment. Such a task cannot be performed for a project of the scope of this feasibility study. Nonetheless, since noise is an important factor in the evaluation of the feasibility of a high gain pneumatic device, the results of other work on high gain pneumatic sensors and amplifiers must be examined in order to determine the probable relationship between noise and the present application.

Noise in a vortex amplifier can generally be traced to turbulence and any steps taken to reduce turbulence in the amplifier will generally reduce noise. The steps that can be taken include reduction of surface roughness, improvement of the efficiency and smoothness of mixing processes, design of entry ports to insure smooth injection of incoming fluids, and elimination of abrupt turns. Amplifier noise may be also reduced by minimizing the total flow through the chamber. Total flow may be reduced by reducing the size of the outlet orifice or by reducing the pressure.

Some idea of the frequency distribution of vortex amplifier noise may be gained by passing the waveform through filters with various time constants. Typical results show that 60 percent of the noise amplitude exists at frequencies above 5 cps.

Vortex amplifier noise originates in either the chamber or the pickoff. Use of hot wire anemometer probes in vortex chambers has indicated that much of the turbulence in the chamber arises at the edge of the button where there is a change in flow direction from axial to radial. There is a distinct reduction in turbulence intensity as the center of the chamber is approached. A swirling component reduces the turbulence and separation at the edge of the button markedly. Other sources of chamber turbulence arise from the manner in which the fluid streams enter the chamber and mix to form the overall velocity field. Careful design and manufacture of inlet ports is of extreme importance here.

The consideration of noise within the pickoff is most complex in nature. The complexity of the three-dimensional flow issuing from the exit makes a mathematical approach to pickoff noise impossible. On the other hand, accurate velocity measurements are impractical, because even the smaller hot wire probes are very large in comparison with the typical outlet hole. Investigation of pickoffs must mainly be concerned with evaluation of various pickoff geometries. In addition, well defined noise generating mechanisms within the pickoff such as edgetones, jet instability, and attachment phenomena can be investigated and eliminated or reduced by using smooth transition boundaries in the pickoff zone.

In addition to the efforts which can be made to improve the noise characteristics of a vortex amplifier through careful internal design and fabrication techniques, there are several approaches to noise reduction which can be made through changes in external circuitry. One of the most obvious of these is to filter out the noise. Unfortunately, a high percentage of the noise is at such a low frequency that any filtering sufficient to significantly reduce the noise level reduces the system response to undesirable levels. Other circuit approaches involve such techniques as cancellation. Here two identical amplifiers are connected in a push-pull configuration. All systematic disturbances are effectively cancelled because the outputs of the two units are connected in opposition. Thus, any change in supply control or vent pressure will provide an equal shift in output of each of the two sensors and the variations will subtract. Application of this technique to the neutron sensor would be made difficult because of the logarithmic output requirement.

The lowest noise levels which have been obtained with vortex devices at Bendix have been on the order of an inch of water (0.036 psi) measured at the output. These were obtained with a 3-in. diameter

vortex amplifier having an external pickoff which was used in a high gain sensor application involving input signals of a low order of magnitude. It should be noted that in this unit all flow entering the vortex chamber passed through a porous element. As a result, the incoming flow was distributed around the circumference of the amplifier in an extremely uniform manner and undoubtedly entered with a minimum of turbulence. Achievement of this low noise level was not accomplished without significant effort to remove geometrical imperfections and misalignments. Careful adjustment of the circuit to achieve optimum operating conditions was also required.

It has been assumed that this noise level can be achieved in the neutron sensor. This assumption is based on a general similarity of the two applications and presumes that the neutron sensor amplifier can have a physical configuration similar to the porous element amplifier. Although porous elements, as such, may not be suited for use in the neutron sensor, an approach to a porous element may be made by using a multiplicity of carefully shaped control ports and inlet straightening vanes. Care must be taken to insure that those precautions do not make the device rate sensitive. It will be of the utmost importance to insure that the incoming flow enters the amplifier with a minimum of turbulence.

Intensive effort is underway to isolate causes of vortex amplifier noise and to discover means of eliminating or reducing noise. Thus, the achievable noise level should tend to decrease in the future.

It should be noted that most work on the study of noise and noise reduction has involved the use of air or nitrogen as the working fluid. There is little or no information available on the effects on noise resulting from the use of hydrogen working fluid. However, as was indicated in Section 5.2.1, the neutron sensor will operate at very much the same Reynolds numbers as a vortex amplifier operating on 30 psig room temperature air or nitrogen. Thus, turbulence characteristics should be equivalent.

Another potentially serious problem, which has already been discussed in Section 5.3.3, and which will require further investigation, is the null shift caused by the nonlinear amplification of noise.

Another effect, related to the noise problem, is that of the shock and vibration sensitivity of vortex amplifier systems. To an extent, elimination of any potential shock and vibration problems is one of design; the neutron detector system, including supply lines and other connections to and from the rocket vehicle, must not have resonances too close to the range of frequencies to which it will be exposed in service. However, if neutron sensor components are unduly sensitive to shock and vibration, design of an isolated system will be difficult. At this writing, the shock and vibration sensitivity of vortex amplifiers is undefined; there does not seem to be great cause for concern, but there is a lack of experimental evidence in this area.

SECTION 6

SENSOR SYSTEM ANALYSIS

6.1 DESCRIPTION OF SYSTEM

6.1.1 EFD Pump

The pump that the study indicates is most feasible is illustrated in Figure 6-1. The structural materials are beryllium for the outer wall and moderator and beryllium oxide for the insulating members. The ribbons used in the grid structure may be any metal that can be spot welded to the beryllium and that is compatible with the high pressure hydrogen at 350°F. One cm is suggested as the pump inside diameter.

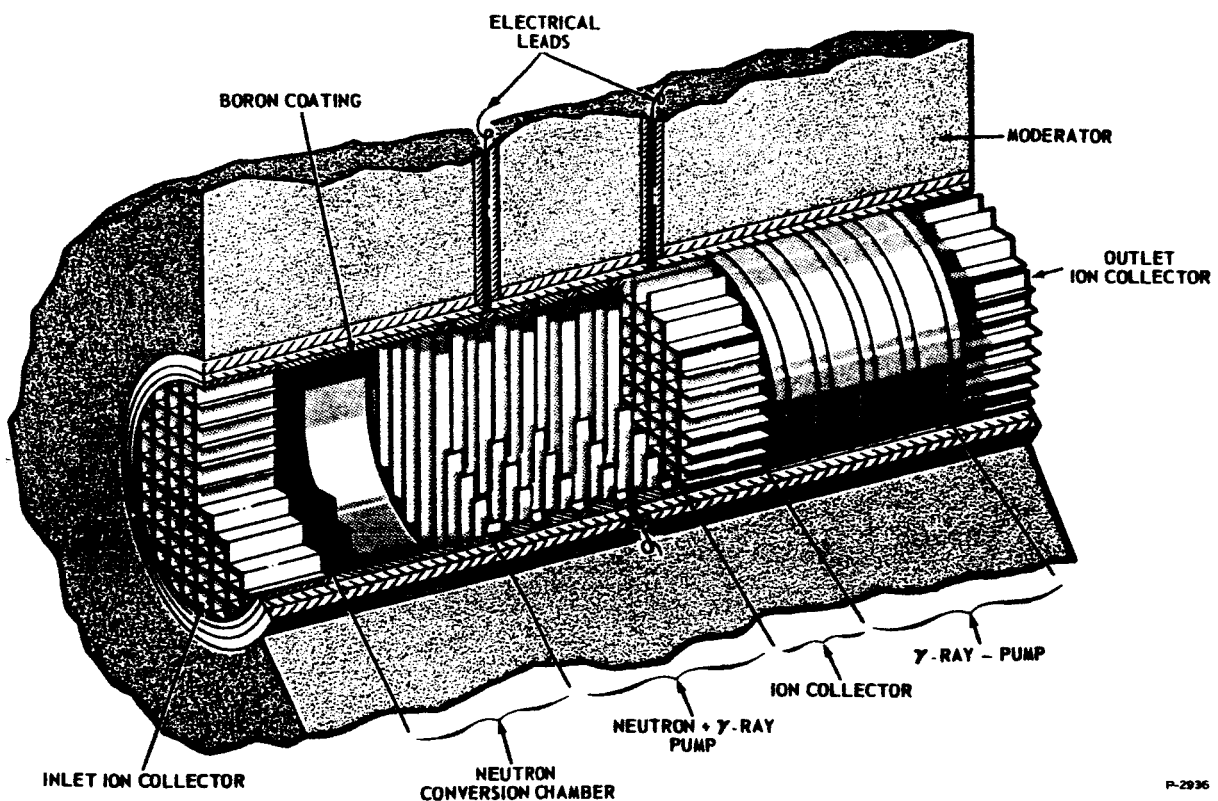


Figure 6-1 - Ion Pump Perspective

P-2936

Ribbon shaped grid members 0.001 in. thick and 0.020 apart are proposed to provide isolation between the electrical fields of the four pump sections.

The inlet to and outlet from the pumps are identical honeycomb or stacked-tube flow straighteners. The primary purpose of the straighteners is to collect free charge carriers. Experiment may prove this is not critical. However, lack of knowledge leads one to anticipate that charge collection is a problem to be solved.

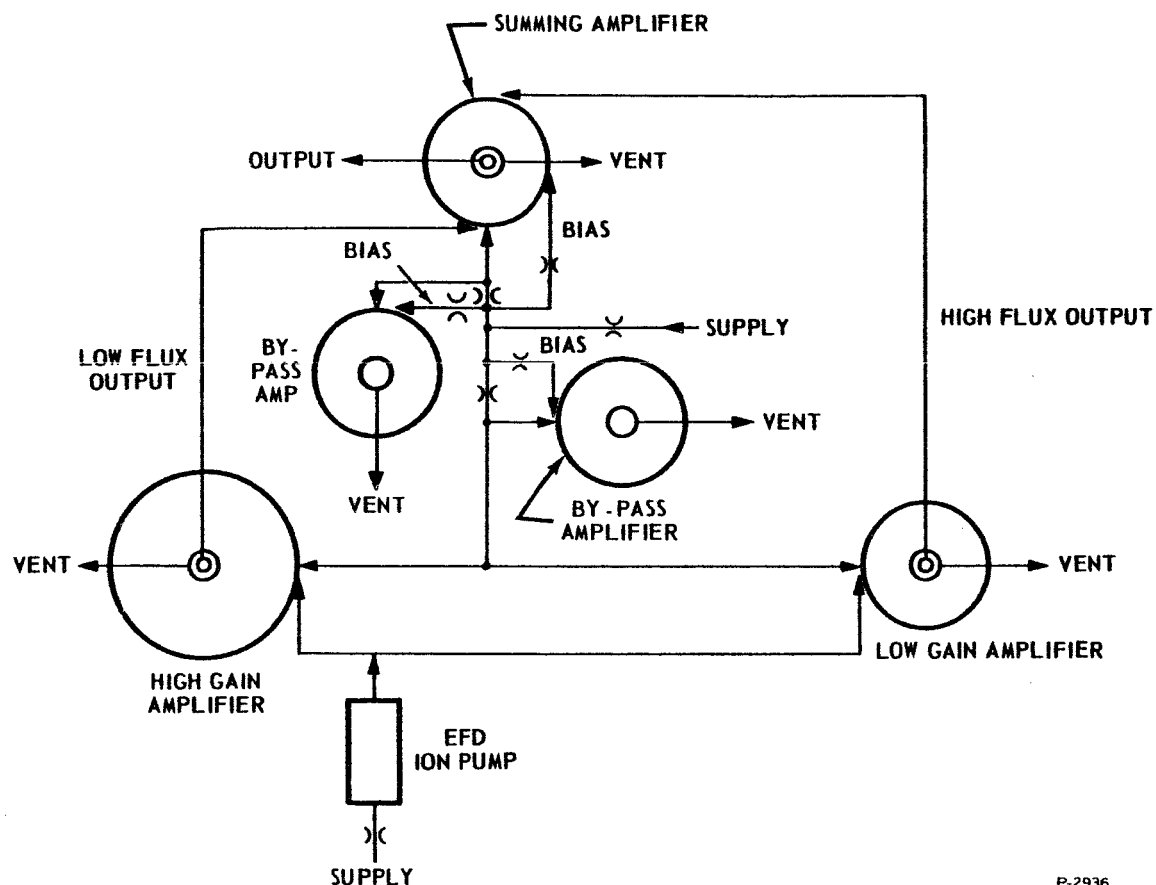
The two pumps are shown with four sections each. The inlet straightener reduces turbulence and provides gas containing a minimum of gamma-ray ionization. The gas is then ionized by neutrons in the boron lined chamber. The gamma-rays also ionize it. The first pump adds a positive differential pressure in the direction of flow. As much of the space charge as possible is collected in the middle honeycomb section. The second pump is polarized to pump against the mean flow and will pump on the gamma-ray ionization density and thereby compensate for at least 90 percent of the gamma-induced ionization.

Balancing for maximum range of gamma-ray compensation can be accomplished by voltage variation of the outlet ion collector. The range will be limited by the nonlinearity of the sensor response. Any additional compensation required will be accomplished by appropriate gamma-ray shielding, as described in Section 6.2.1.

6.1.2 Vortex Amplifiers

Figure 6-2 shows a schematic of the pneumatic circuitry of the neutron detector. A system with the maximum number of components is indicated. An actual system might have a lesser number of components. The actual number will depend upon the ability of the combination of the EFD ion pump and vortex amplifier to produce a logarithmic function for a given number of decades of input and also upon the type of load supplied by the neutron sensor. Under the proper conditions, the neutron sensor could consist of the ion pump and a single high gain vortex amplifier.

The schematic shows a single ion pump driving both the low flux range and the high flux range amplifiers. This is feasible because of the fact that, if the ion pump were perfectly linear, a maximum gain of 3 for the low gain vortex amplifier would be required. Since gains much higher than this are easily obtained, the ion pump and its supply orifice may be operated near saturation in the input range of the low gain amplifier.



P-2936

Figure 6-2 - Pneumatic Neutron Flux Detector Schematic

The high gain amplifier will have a vortex diameter no greater than three inches while the low gain amplifier will have a vortex diameter no greater than one inch. If the three-inch amplifier is designed to have a maximum gain of approximately 3000, it may be operated over four decades of input. The low gain amplifier may be operated over at least two decades of input. If the ion pump were perfectly linear, the vortex amplifier gains to give a near-logarithmic output would be as shown in Table 6-1. In order to achieve the full range indicated, the high gain vortex amplifier will be essentially linear over at least its first decade of input.

The schematic of Figure 6-2 provides for the use of by-pass pressure regulating amplifiers. These are used to remove excess supply flow as the control flow of the pressure amplifiers increases. They also may be used to help shape the final output into the desired logarithmic function through proper selection of the initial operating points. These amplifiers would be in the 1- to 2-inch diameter range.

Table 6-1 - Desired Vortex Amplifier Gains for Linear Ion Pump

Decade	Range of Pressure Gains	Amplifier
1	3000 - 3000	3 inch
2	3000 - 300	3 inch
3	300 - 30	3 inch
4	30 - 3	3 inch
5	3 - 0.3	1 inch
6	0.3 - 0.03	1 inch

The outputs of the two primary amplifiers will be summed in a one-inch vortex amplifier. This amplifier will also serve the purpose of impedance matching between the primary amplifiers and the load. Even if the nonlinear characteristics of the ion pump permitted the use of only one primary amplifier, an impedance matching amplifier would be required if the neutron sensor is required to drive a load having significant flow demand.

The temperatures to which the neutron sensor will be exposed are moderate. The maximum temperature of 800°R (340°F) is well within the range at which various aluminum alloys have useful strength. There are a number of aluminum alloys which have stress-to-rupture values of 27000 psi after 100 hours exposure to temperatures of 400°F. These include alloys 2020-T6, 2024-T81, 2219-T81, and 2618-T61. For a 5-inch diameter cylinder with 150 psig internal pressure, wall thickness must be reduced to 0.014 inch before a stress of 27000 psi is reached. Thus it can be concluded that aluminum is sufficiently strong for this application. Use of aluminum is also advantageous from the point of light weight and low gamma heating.

6.1.3 Complete System

The vortex amplifier circuitry may be visualized as consisting of a manifold, which would comprise a block or plate to which the various vortex amplifiers would be fastened. The fluid connections between the vortex amplifiers would be drilled channels through the manifold. The ion pump can connect directly into the high gain amplifier in order to obtain as close a coupling as possible. If a low gain amplifier was to be driven off the ion pump also, its input could be drawn off the supply annulus of the high gain amplifier. Figure 6-3

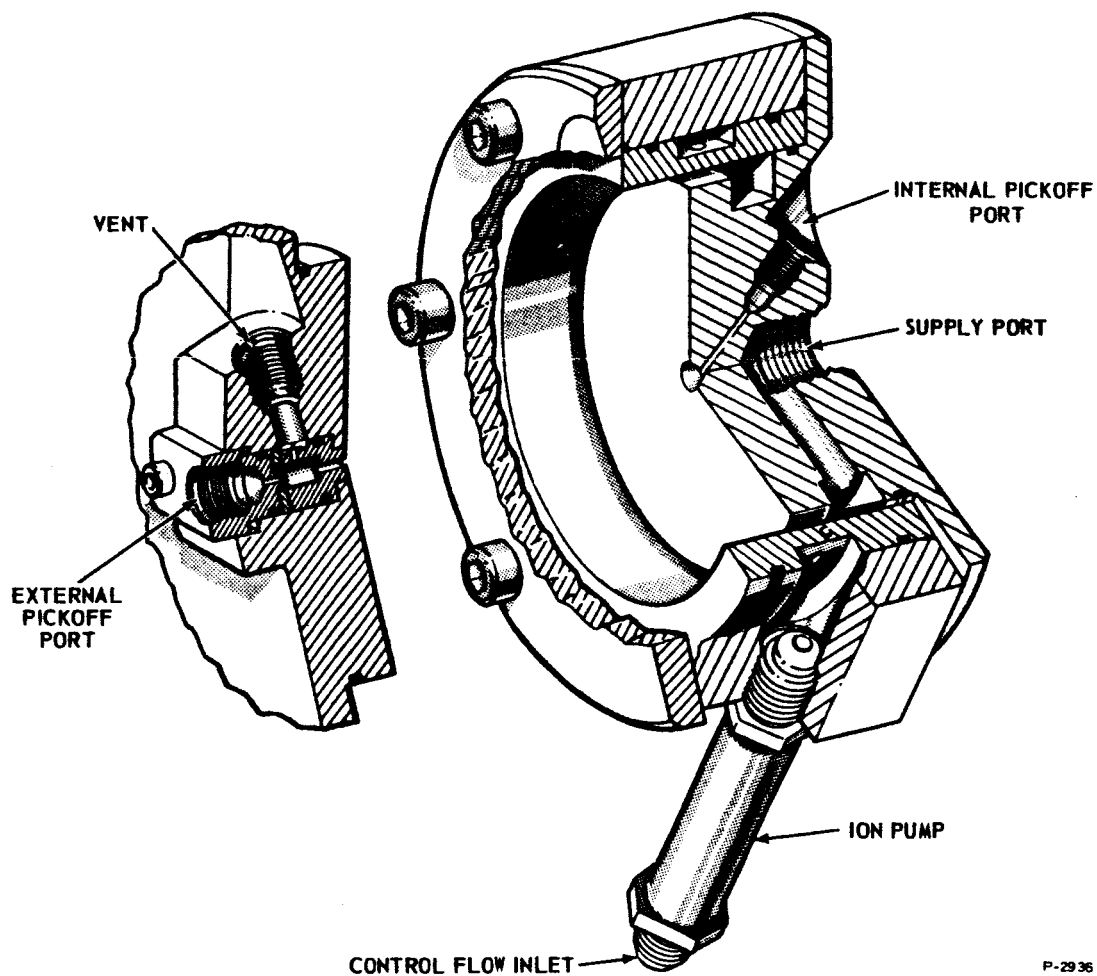
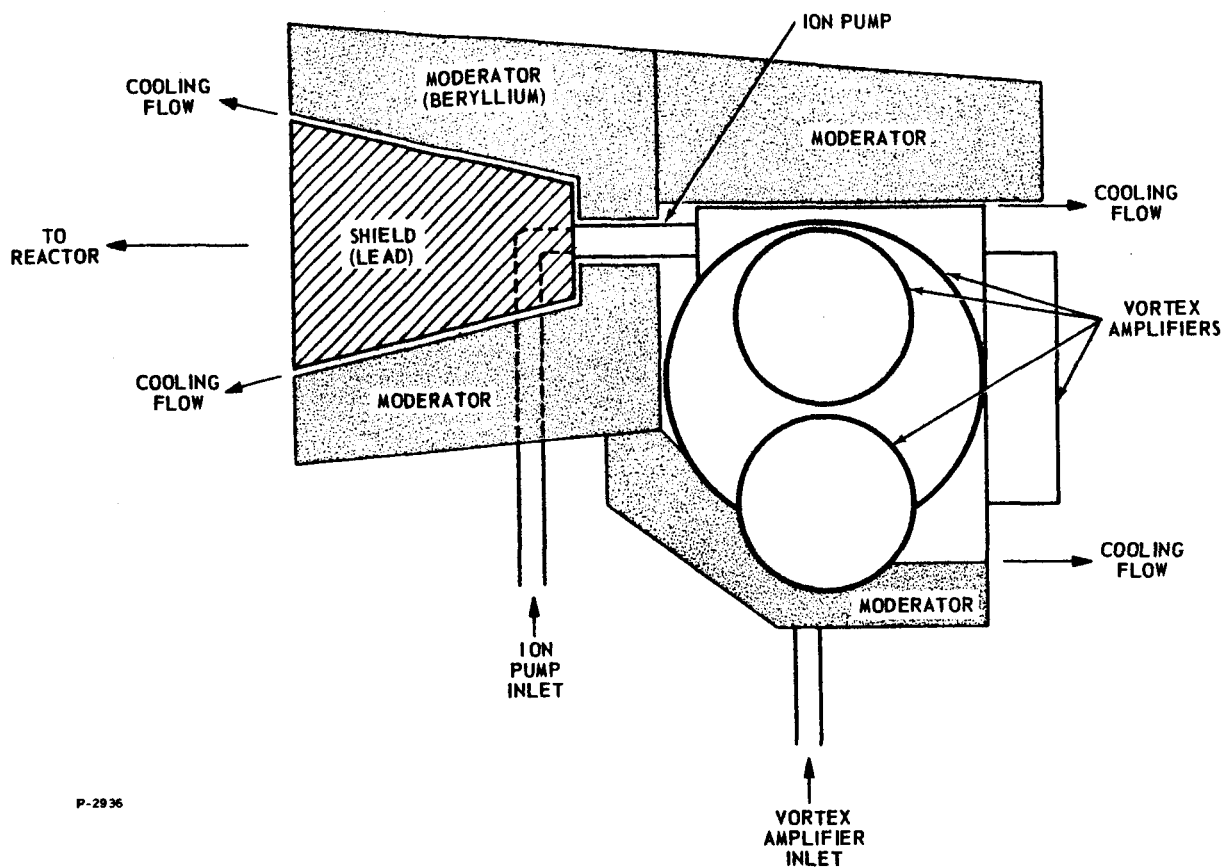


Figure 6-3 - Ion Pump-Vortex Amplifier Assembly

illustrates the connection between the ion pump and the high gain amplifier and also indicates the constructional features of a vortex amplifier.

The overall arrangement of the system, specifically indicating the relationship between the shield, moderator, ion pump, and vortex amplifier system, is shown in Figure 6-4. The shield is of lead in the shape of the frustum of a cone which has a solid angle which prevents the ion pump from "seeing" all of the gamma flux. The moderator surrounds the ion pump in all directions except at the ends. The vortex amplifier system is not symmetrical with the ion pump and the shield, and some awkwardness in applying moderator around this part of the system results. If parts of the vortex amplifier system can be made of beryllium, a cleaner design will be possible. It can be ques-



P-2936

Figure 6-4 - Shield and Moderator Schematic

tioned whether it is practical to make the vortex amplifiers entirely out of beryllium, but it is likely that the manifold and some of the other structure within the vortex amplifier system can be fabricated from this material. This will ease problems in applying moderator around the vortex amplifier system considerably.

The exhaust from the vortex amplifier system will be passed around the moderator and shield for purposes of cooling. The moderator and shield should be mounted in a manner that thermally isolates them as completely as possible from the ion pump and the vortex amplifier module.

The shield will be 2.5 in. thick. The diameter of the moderator on the surface facing the reactor will be approximately 7 inches. The outside diameter of the largest vortex amplifier will be approximately 5 inches.

6.2 NUCLEAR STUDIES

6.2.1 Gamma Shielding

The criterion for whether gamma shielding is required and the amount that will serve a useful purpose is that the minimum compensated signal must be ten times as large as that caused by gamma-ray ionization of the gas at its maximum density. The worst condition for gamma compensation is during a restart because the gamma radiation will decay at a much slower rate than the neutron radiation. The ratio of residual gamma flux to neutron flux can therefore vary widely depending on the ratio of reactor operating time to shut-down time. This analysis assumes a maximum of 20 minutes operating time and minimum shutdown of 30 minutes. The estimated residual gamma flux is 5×10^7 ergs $\text{gm}^{-1} \text{hr}^{-1}$ which will generate 4×10^{11} ion pairs $\text{cm}^{-3} \text{sec}^{-1}$. Since the opposing pumps provide acceptable compensation of at least a factor of ten, the minimum compensated signal is that required to produce 10^{-4} psia, namely, a charge density of $6 \times 10^9 \text{ cm}^{-3}$. The gamma flux reduction required of the shield is therefore a factor of 67. This is accomplished by six half thicknesses of shadow shielding for the direct flux. Side shielding is not required since the scattered gamma component will be significantly reduced in energy and hence will not contribute greatly to the total ionization. 0.42 in. of lead or 0.9 in. of steel is a half layer for 1 Mev gamma rays. A lead shadow shield in the form of a truncated cone is shown in the drawing of Figure 6-4. Coolant passages within the shield are provided to prevent excessive temperatures due to the gamma heating.

The auxiliary pneumatic components may also be used for shielding as long as they are unaffected by gamma heating.

6.2.2 Gamma Heating

The interaction of radiation with matter results in the transfer of the radiation energy to heat energy within the exposed material. Of the various nuclear radiations from the reactor, only the neutrons and gamma photons need to be considered as sources for generating heat. It is during the process of slowing down that these radiations lose energy and thus generate heat in the surrounding material.

The rate of gamma energy deposition in a material assuming no self-shielding is given by:

$$q_{\gamma} = K \frac{\mu_a}{\rho} \phi_{\gamma} \quad (6-1)$$

where

q_{γ} = gamma heating rate, B/lb-hr

K = conversion factor = $2.48 \times 10^{-10} \frac{\text{B-gm-sec}}{\text{Mev-lb-hr}}$

μ_a/ρ = gamma energy absorption coefficient, cm^2/gm

ϕ_{γ} = gamma energy flux at surface of material, $\text{Mev}/\text{cm}^2\text{-sec}$

The expected gamma flux is 5×10^9 ergs/gm hr, which is equivalent to 3.1×10^{13} Mev/ $\text{cm}^2\text{-sec}$. Substituting this value in equation (6-1) with the appropriate gamma energy absorption coefficients gives the following values for q_{γ} .

Beryllium	166 B/lb-hr
Aluminum	189 B/lb-hr

Dividing q_{γ} by the specific heat of the materials yields the materials' adiabatic temperature increases, which are 390°F/hr for beryllium, 820°F/hr for aluminum, and 1200°F/hr for a lead shield which absorbs all the γ -flux in a 130 cm^2 cross-sectional area.

Neutron heating in metals is usually insignificant, compared to the gamma heating, but depends of course on the neutron-to-gamma ratio of the incident environment. For the neutron-to-gamma ratio specified, the contribution of neutrons to the total heating rate is expected to be less than 1.0 percent.

The neutron sensor system weight estimates are given in Section 6.6. If it is assumed that the system will consist of 8.5 lbs of aluminum, 5.5 lbs of lead and 15.2 lbs of beryllium, the total heat generation within the neutron sensor will be 4300 B/hr. Also from Section 6.6, the estimated hydrogen flow through the neutron sensor will be 0.0082 lb/sec = 29 lbs/hr at 800°R. The specific heat of hydrogen at 800°R is 3.5 B/lb°R. The flow through the neutron sensor will thus be capable of absorbing the internal heat load with a temperature rise of

only 42°F. This will be acceptable, since the major heating load that is represented by the shield and moderator will be absorbed by the gases after they have passed through the ion pump and vortex amplifiers. Since the moderator and shield will be the components having the greatest gamma heating and may therefore reach temperatures higher than the rest of the system, measures to contain them and to isolate them thermally from the ion pump and vortex amplifier should be taken.

In the event that the hydrogen flow required to supply the neutron sensor is not as high as the estimate made in Section 6.6, as would happen if a lesser number of vortex amplifiers was used, some additional hydrogen for moderator and shield cooling might be required. However, the total hydrogen flow required will not be in excess of that already estimated in Section 6.6.

6.2.3 Moderator

A moderator is required to thermalize the fast neutron flux for maximum conversion of neutron flux to ionization. Criteria for the moderator are minimum size and weight, compatibility with the environment and other materials used with the sensor, and minimum attenuation of the neutron flux. Candidate materials that show promise of meeting these criteria are beryllium, carbon, hydrogen and polystyrene. A list of the pertinent properties of these materials is given in Table 6-2.

The best measure of the moderating capability is the slowing down length and the moderating ratio. The slowing down length is the average distance traveled by a fission neutron in slowing down to thermal

Table 6-2 - Moderating Characteristics of Various Materials

Moderator	Density g/cm ³	Scattering Cross Section cm ⁻¹	Slowing Down Length cm	Absorption Cross Section cm ⁻¹	Moderating Ratio
Beryllium	1.84	0.55	9.9	0.0011	150
Carbon	1.62	0.30	18.7	0.00037	170
Hydrogen liquid	0.07	0.168	15	0.014	12
Polystyrene	0.9	0.31	8.1	0.025	12

P-2936

energy. This distance roughly represents the length of moderating material the fast neutrons should pass through before reaching the neutron sensitive coating. This value should, of course, be as low as possible.

The moderating ratio is the ratio of the slowing down capability to the thermal neutron absorption cross-section. Since it is desirable for the thermal neutron absorption to be as low as possible the larger the moderating ratio the better.

Beryllium has the best combination of slowing down length and moderating ratio, as shown in Table 6-2, and is therefore recommended as the moderator. Polystyrene has a comparable slowing down length and with its lower density would weigh only half as much as the beryllium moderator. However, polystyrene has a greater thermal neutron absorption cross-section; so the thermal flux at the detector would be lower. It also has the disadvantage of being radiation and temperature sensitive. The material could be canned with a relief valve to relieve the off-gassing and cooled to prevent excessive temperatures.

Two other materials that have comparable slowing down properties to the beryllium but which also have greater thermal neutron attenuation are polyethylene and lithium hydride. These materials would offer some reduction in weight at the expense of neutron flux attenuation. However, polyethylene does not have the temperature and radiation resistance of polystyrene.

The estimated neutron flux attenuation by beryllium is less than 2 percent while the polystyrene reduces the flux by approximately 30 percent assuming simple exponential attenuation of a monoenergetic beam through a thin slab. Since the weight penalty for beryllium was preferred over the attenuation of neutron flux, beryllium was selected. The configuration shown in Figure 6-4 is based on inserting between the pump and the reactor in all directions a minimum moderator length equal to the slowing down length. This has been accomplished except for the front face where the shield is located, the back face where the vortex amplifiers and manifold are located and for a small segment at right angles to the pump. It was decided that the weight savings obtained by minimizing moderator in these areas was worth the small loss in thermal flux. It is estimated that the total reduction in thermal neutron flux by the shield and lack of complete thermalization in all directions is slightly over 10 percent. This is because both the shield and vortex amplifiers provide some moderation and the scattered flux impinging on the rear face is already degraded significantly in energy.

The moderator design is not a critical one since any type of neutron sensor will require a similar moderator -- only the shape may differ. Also, the location of the sensor, the surrounding materials and detailed flux spectrum can alter the moderator design significantly. Hence, the moderator configuration shown in Figure 6-4 should be regarded as a representative design rather than a final one.

6.2.4 Neutron Conversion Coating

The analysis performed on the EFD pump was made on the basis of a Boron-10 coating for converting the thermal neutron flux to a charged particle flux which has much greater ionizing capability. An alternate conversion coating which can be considered for use with the pump is a fissionable material such as Uranium-235. When a thermal neutron produces a fission in U^{235} , nearly 200 Mev of energy from fission fragments is released to the gas in comparison to the 2 Mev released from the n- α reaction in B^{10} . However, the total amount of ionization produced in the gas is also a function of the number of ionizing particles produced per unit neutron flux.

A comparison of the ionizing capability of each type of conversion coating can be made by ratioing the amount of ionization produced per unit neutron flux in a given volume of gas by each type of coating. The ionization produced in the gas from thermal neutron flux interactions in the conversion coating is given by:

$$n_i = \frac{2 \phi_n \zeta R Q \Gamma X}{M v_g} \quad (6-2)$$

where

X = length of pump

ζ = fraction of total possible ionization produced by the released particles in the gas

Γ = total ionization per particle per range

The ratio of B^{10} to U^{235} ionization is therefore

$$\frac{n_{iB}}{n_{iu}} = \frac{\zeta_B R_B Q_B \Gamma_B M_u}{\zeta_u R_u Q_u \Gamma_u M_B} \quad (6-3)$$

where subscript B refers to B¹⁰ and U to U²³⁵. Evaluating the ratio with the quantities:

$$\zeta_B = \zeta_u$$

$$R_B = R_u - \text{optimum mass thickness is nearly identical}$$

$$Q_B = 4 \times 10^3 \text{ barns}$$

$$Q_u = 5.5 \times 10^2 \text{ barns}$$

$$\Gamma_B = 5 \times 10^4 \text{ ions per } \alpha \text{ particle}$$

$$\Gamma_u = 8 \times 10^5 \text{ ions per fission fragment}$$

$$M_B = 10M_H \text{ assuming fully enriched B}^{10}$$

$$M_u = 235M_H \text{ assuming fully enriched U}^{235}$$

gives

$$\frac{n_{iB}}{n_{iu}} = 10$$

For U₃O₈, the compound usually employed in fission chambers, the ratio is even greater in favor of B¹⁰.

In either case the B¹⁰ coating produces the greater amount of ionization per unit flux and it has the further advantage of avoiding the handling and use of radioactive materials; so B¹⁰ is the recommended neutron sensitive coating for the EFD sensor.

Engineers from Westinghouse, Electronic Tube Division, Elmira, New York, confirmed in various telephone conversations that B¹⁰ coating could be deposited on very small surfaces of odd-shaped objects and on various materials, including beryllium, titanium, aluminum, etc. The process is a well-established one and is used exclusively on the Westinghouse tiny 1/4" flux mappers. The process is essentially one of painting on the coating with a binder and subsequently baking off the binder. No particular problems are contemplated for the neutron sensitive coating even over the full operating temperature range since Westinghouse has tested the coatings over greater ranges.

6.3 SYSTEM DYNAMIC RESPONSE

The desired neutron sensor time constant is 0.02 sec for neutron flux values greater than 10^7 neutrons/cm² sec. This is equivalent to a 95 percent response time of 0.06 sec.

Estimates made in Section 5 show that a high gain vortex amplifier whose design is equivalent to an existing 3-in. diameter device will have a response time of less than 0.07 sec when operating on 200°R hydrogen. The response can be improved by increasing the flow rate through the vortex chamber, which for a given supply pressure, can be accomplished by increasing the area of the outlet orifice. This change, if not offset by other modifications, will result in a loss in gain. One such change would be to operate the vortex amplifier with a high ratio of control flow to outlet orifice flow which acts to increase pressure gain. By properly balancing the two effects, it will be possible to achieve response times less than 0.06 sec while maintaining gains high enough to obtain a useful range.

If, as is likely, the high gain amplifier is used to drive another vortex amplifier used for signal summing or impedance matching, significant dynamic lags will be introduced. As indicated in Section 5, these should be no greater than that represented by a 0.01 sec time constant and may be considerably less, depending upon the flow demand of components downstream from the neutron sensor. There should be an adequate margin of gain in the larger vortex amplifier to permit the achievement of the desired response in the overall system. As gas temperature increases above 200°R, dynamic response requirements can more easily be met.

Dynamic response in the ion pump section will depend upon two physical effects: the stay time in the ion pump and the compressibility of the gas volume between the ion pump and the vortex amplifier control ports. In view of the relatively large gas flow through the ion pump, the gas volume compressibility will not be significant. The stay time in the ion pump will be determined by the effective length for ionization divided by the gas velocity. Assuming a neutron conversion chamber length of 1 cm and a gas velocity of 4 meters/sec gives a staytime of 0.0025 sec.

6.4 SYSTEM RANGE

In Section 5 it was shown that a high gain vortex amplifier used in the neutron sensor application would have a maximum pressure gain

in the range of 3000 to 6200. It was also noted that noise levels as low as one inch of water measured at the output had been achieved with a three-inch vortex amplifier used in another high gain sensor application. The exact configuration of the amplifier in which this low noise level was achieved is somewhat different from the amplifiers which would be used in the neutron sensor. However, it has been assumed that this noise level can be achieved in this application by means of careful design and precise construction techniques.

Dividing the minimum expected noise level by the maximum gain gives the minimum signal input which can be detected over the noise level. Dividing 0.036 psi, which is the equivalent of one inch of water, by 3000, gives a minimum detectable input pressure change of approximately 10^{-5} psi.

From the results given in Section 4, it can be shown that an ion pump output pressure rise of 10^{-5} psi is equivalent to a thermal neutron input of approximately 1.7×10^6 neutrons/cm² sec. There will be some loss in the conversion of fast neutrons to thermal neutrons. However, we can conclude that at least five complete decades of fast neutron flux from 10^7 to 10^{12} neutrons/cm² sec can be measured.

Any investigation of methods of achieving greater ranges with the electrofluidynamic neutron sensor would require an experimental effort. However, it can be concluded that achieving the desired goal to ten decades with a device of this type will be difficult.

6.5 SYSTEM ACCURACY

There are a number of aspects to estimation of the accuracy of the neutron sensor. Some of these are as follows:

- (1) The ability of the neutron sensor to produce the desired logarithmic relationship between the neutron flux and the output pressure.
- (2) The sensitivity of the neutron sensor to environmental and supply conditions.
- (3) The ability of the device to discriminate between neutron and gamma flux as discussed in Section 6.1.1

The accuracy with which the device meets the desired logarithmic curve describing the output pressure in terms of the neutron flux is largely a problem of calibration. However, since the output of the device

is not a mathematically generated function of log neutron flux but is instead a matching of the natural nonlinear characteristics of the overall system with the desired logarithmic curve, the actual output will always deviate from the ideal. The point of greatest deviation will occur at the lowest input signal level and will be a consequence of the device being essentially linear rather than logarithmic at the lower ranges. If the overall system is linear over the lowest decade, the greatest error, expressed as a percent of the total output pressure range, will be $61/N$ where N is the number of decades of input. For five decades of input, then, the percent error at the lowest input signal will be approximately 12 percent. Over the rest of the operating range, the estimated deviation from the ideal logarithmic curve should be no greater than 5 percent of the output pressure range.

The inaccuracies resulting from the deviation of the actual output curve from the ideal logarithmic curve will be consistent. As a result, the deviations can, to an extent, be compensated in downstream components.

The inaccuracies resulting from sensitivity to changes in supply and environmental conditions relate almost solely to changes in pressure, temperature, or voltage. Changes in ambient pressure can be ignored since the pressure level in the neutron sensor will be high enough to assure that the pressure ratio across all vents will be less than the critical value even at one atmosphere back pressure.

The consequences of a change in supply pressure are potentially more serious, since a change in supply pressure will change pressures proportionately throughout the system. Thus, a given percentage shift in supply pressure will cause the same percentage shift in output pressure. The neutron sensor system can be no more accurate than the accuracy of its supply pressure regulation. The neutron sensor system will represent a fairly constant flow demand so that the effect of the sensitivity of the pressure regulator to flow will be minimized. The effect of variations in the hydrogen storage pressure can, if necessary, be minimized through the use of a two-stage pressure regulator. Temperature sensitivity and random variations in regulated pressure will be much more significant. All possible precautions in the design and placement of the pressure regulator should be taken to minimize these effects. In addition, any other fluid-state circuits operating in conjunction with the neutron sensor in the overall reactor control loop should be supplied from the same regulator in order that shifts in the regulated pressure affect all subsystems equally. This will eliminate the possibility of two different regulated pressures shifting in opposite directions. However, the output

pressure of the overall fluid state system will shift in proportion to any shift in regulated pressure.

The voltage sensitivity of the pump is such that one half of any relative change in voltage will appear in the opposite direction as a relative change in pressure. The power supply should have a stability of the order of 1 percent, a requirement that is easily met.

The most serious potential source of error is that which results from shifts in supply gas temperature and ambient temperature. Changes in temperature not only affect the static performance of vortex amplifiers but may also cause changes in the regulated supply. The temperature sensitivity of vortex pressure amplifiers is an area requiring further investigation. In Section 5 it was shown that the simple vortex amplifier is sensitive enough to temperature that some form of temperature compensation will be required if the hydrogen supplied to the sensor varies over the full 200 to 800°R temperature range. This compensation may be provided in the individual amplifiers or by some additional fluid-state circuitry, depending on the severity of the shift. If the hydrogen flow to the neutron sensor can be maintained at a constant or near-constant temperature, the need for compensation can be minimized.

6.6 SYSTEM WEIGHT AND GAS CONSUMPTION ESTIMATES

The high gain vortex amplifier may be assumed to be a cylinder 4.0 in. in diameter by 2.0 in. long. The volume of such a cylinder is 25 in.³. It can be assumed that a vortex amplifier is at least 20 percent void. Then an aluminum (density 0.1 lb/in.³) three-inch diameter vortex amplifier will weight approximately two pounds. A two-inch diameter vortex amplifier may be assumed to be a three-inch diameter cylinder 2.0 inches long. It may thus be estimated at 1 lb. A one-inch vortex amplifier may be assumed to be 2.0 in. diameter by 1.5 long and thus will weigh approximately 0.5 lb. The manifold connecting the amplifiers together, including provision for fastening and plumbing, should weigh no more than the largest amplifier. Then, adding the weights on one three-inch diameter amplifier, one two-inch amplifier, three one-inch amplifiers, and a manifold gives an estimated weight of 6.5 lbs for the vortex amplifier system.

The ion pump is basically a hollow tube 1/2 in. in diameter by 2-1/4 in. long. Allowing a weight of 0.2 lb for this component seems adequate. The shield is the frustum of a cone which is 2.5 in. high having base diameters of approximately 3.2 and 2 in. This gives a weight of

approximately 5.5 lbs. The moderator weight is estimated as 15 lbs on the basis of a beryllium tube 3.5 in. I.D. x 6.0 in. O.D. x 12 in. long.

The total estimated weight of the neutron system including an allowance for connection and mounting is

Vortex amplifier module	6.5 lb
Ion pump	0.2
Shield	5.5
Moderator	15.0
Allowance for connections and mounting	2.0
	<hr/>
Total estimated dry weight	29.2

The gas consumption may be estimated by summing the flows of all the vortex amplifier outlets for the maximum output pressure of 150 psia. For a 3-in. diameter vortex amplifier with a 0.090-in. diameter outlet orifice, the outlet flow will be 0.006 lb/sec of hydrogen at 200°R. The 2-in. pressure regulating amplifier may have an outlet orifice of the same size and hence will have a similar flow demand. The 1-in. amplifiers may have outlet orifices with areas one quarter that of the larger amplifiers and may be rated at a flow of 0.0015 lb/sec. (This is conservative since the summing amplifier will actually operate at reduced supply pressure.) Adding the estimated hydrogen flow of 0.006 lb/sec for each of the two larger amplifiers to the 0.0015 lb/sec for each of the smaller amplifiers gives a total estimated flow of 0.0165 lb/sec of hydrogen at 200°R. At 800°R, the total hydrogen flow will be 0.00825 lb/sec.

APPENDIX A

NOTATIONS

A-1 NOTATION FOR EFD PUMP ANALYSIS

a	= Recombination rate - $\text{cm}^3 \text{ sec}^{-1}$
α	= Subscript denoting "a-particle"
β	= Coefficient in definition of field dependent mobility ($\text{M}^3 \text{ Atm}^2 \text{ volt}^{-2} \text{ sec}^{-1}$)
b	= Charge carrier mobility ($\text{M}^2 \text{ volt}^{-1} \text{ sec}^{-1}$)
B	= Magnetic induction (Webers M^{-2})
δ	= Mass density (Kg M^{-3})
e	= Subscript denoting "electron"
E	= Electric field (Volts M^{-2})
ϵ	= Permittivity (FM^{-1})
f	= Subscript denoting "fluid"
ζ	= Fraction of total possible ionization
F	= Force per unit volume (Newtons M^{-3})
i	= Subscript denoting "ion"
j	= Current density (Amp M^{-1})
Γ	= Total ionization per particle per range
m	= Subscript denoting "molecule"
M	= Mass (Kgm M^{-3})
n	= Charge carrier density (M^{-3})
o_n	= Symbol for neutron
o	= Subscript denoting "boundary value" or "measurement condition"
π	= 3.1416
p	= Pressure (Newton M^{-2})

q	= Electric charge (coulombs)
Q	= Microscopic cross-section (M^2)
ρ	= Charge density (Coulomb M^{-3})
r	= Ion pair production $cm^{-3} \text{ sec}^{-1}$
R	= Range (meters)
σ	= Electrical conductivity ($ohm^{-1} M^{-2}$)
t	= Time (sec)
ϕ	= Flux ($M^{-2} \text{ sec}^{-1}$)
v	= Velocity (M/sec^{-1})
V	= Potential (volts)
x	= Coordinate dimension
y	= Coordinate dimension
z	= Coordinate dimension

A-2 NOTATION FOR VORTEX AMPLIFIER ANALYSIS

A_c	= Control port area = $\pi D_c^2/4 - in^2$
A_{oi}	= Internal pickoff tap area = $\pi D_{oi}^2/4 - in^2$
A_2	= Outlet orifice area = $\pi D_2^2/4 - in^2$
C_{dc}	= Control port flow coefficient - dimensionless
C_{di}	= Internal pickoff tap diameter flow coefficient - dimensionless
C_{d2}	= Outlet orifice flow coefficient - dimensionless
D_c	= Control port diameter (see Figure 4-1) - in
D_o	= Pickoff diameter - in
D_{oi}	= Internal pickoff diameter (see Figure 4-1) - in
D_{oe}	= External pickoff diameter (see Figure 4-1) - in
D_1	= Vortex diameter (see Figure 4-1) - in
D_2	= Outlet orifice diameter (see Figure 4-1) - in

g	= Standard gravitational acceleration = 386 in/sec^2
h	= Transport delay - second
h_{max}	= Maximum value of h - second
k	= Ratio of specific heats - dimensionless
K	= Gain in equation (4-50) - psi-sec/lb
K_c	= Constant defined by equation (4-1)
K_i	= Ion pump gain - $\text{psi-cm}^2\text{-sec/neutron}$
k_o	= Outlet flow slope - in^2/sec
K_p	= Pressure gain = $\Delta p_{oi}/\Delta(p_c - p_s)$ - dimensionless
$K_{p\text{max}}$	= Maximum value of K_p - dimensionless
K_v	= Gain defined by equation (4-20) - dimensionless
K_w	= Ratio of control flow to outlet flow - dimensionless
l	= Vortex chamber length - in
m	= Molecular weight - lb/lb-mole
M	= Mach number - dimensionless
n	= Parameter in equation (4-3) - dimensionless
N	= Number of decades of neutron flux to be detected = $\log(\phi_{\text{max}}/\phi_{\text{min}})$ - dimensionless
N_R	= Reynolds number - dimensionless
p_L	= Linear pressure change - psid
p	= Pressure - psia
p_B	= Bias pressure - psia
p_B'	= Pressure regulator bias pressure - psia
p_c	= Control pressure - psia
p_{co}	= Steady-state value of p_c - psia
p_e	= Vortex amplifier exhaust pressure - psia
p_o	= Output pressure - psia
p_{oi}	= Output pressure of internal pickoff - psia

$p_{oi_{max}}$	= Maximum value of p_{oi} - psia
$p_{oi_{min}}$	= Minimum value of p_{oi} - psia
p_p	= Ion pump output pressure - psid
p_{pmin}	= Minimum value of p_p - psid
p_s	= Vortex amplifier supply pressure - psia
p_u	= Upstream pressure defining flow through outlet orifice - psia
p_v	= Average pressure in vortex chamber - psia
p_{vo}	= Quiescent value of p_v - psia
r	= Radius - in
r_i	= Inner radius of vortex - in
r_w	= Outer radius of vortex - in
R	= Ideal gas constant = $18500/m - lb_m in/^{\circ}R lb_f$
t	= Time - seconds
t_R	= Response time - seconds
T	= Absolute temperature - $^{\circ}R$
v_c	= Vortex amplifier control velocity - fps
v_T	= Tangential velocity - fps
v_{T1}	= Tangential velocity at radius r_1 - fps
v_{T2}	= Tangential velocity at radius r_2 - fps
v_w	= Tangential velocity at chamber wall - fps
V	= Volume of vortex chamber - in^3
V_c	= Volume of connecting channel - in^3
W_o	= Outlet flow intercept - lb/sec
\dot{w}_c	= Vortex amplifier control flow - lb/sec
\dot{w}_c'	= Pressure regulator control flow - lb/sec
\dot{w}_o	= Vortex amplifier outlet flow - lb/sec

\dot{w}_o'	= Pressure regulator outlet flow - lb/sec
\dot{w}_{oo}	= Quiescent flow from outlet - lb/sec
\dot{w}_{oi}	= Flow through output pressure tap - lb/sec
\dot{w}_s	= Vortex amplifier supply flow - lb/sec
\dot{w}_s'	= Pressure regulator supply flow - lb/sec
\dot{w}_w	= Flow entering vortex chamber at outer radius - lb/sec
μ	= Dynamic viscosity - lb _m /sec-in
ρ	= Mass density - lb-sec ² /in ⁴
τ	= Time constant - sec
ϕ	= Neutron flux - neutrons/cm ² sec
ϕ_{\min}	= Minimum value of ϕ - neutrons/cm ² sec
ϕ_{\max}	= Maximum value of ϕ - neutrons/cm ² sec
ω	= Angular velocity - radians/sec